Carbohydrate Polymers 157 (2017) 447–467

Contents lists available at ScienceDirect

Carbohydrate Polymers

journal homepage: www.elsevier.com/locate/carbpol

Applications of bacterial cellulose as precursor of carbon and composites with metal oxide, metal sulfide and metal nanoparticles: A review of recent advances

M.L. Foresti [a,b], A. Vázquez [a,b], B. Boury [c,*]

[a] Instituto de Tecnología en Polímeros y Nanotecnología (ITPN), Facultad de Ingeniería, Universidad de Buenos Aires, Las Heras 2214, CP 1127AAR Buenos Aires, Argentina
[b] Consejo Nacional de Investigaciones Científicas y Técnicas (CONICET), Argentina
[c] ICG-CMOS UMR 5253, Université Montpellier 2, Place Eugène Bataillon CC 1702, 34095 Montpellier Cedex 05, France

ARTICLE INFO

Article history:
Received 22 June 2016
Received in revised form 1 September 2016
Accepted 3 September 2016
Available online 14 September 2016

Keywords:
Bacterial cellulose
Carbon
Metal oxides
Metal sulfides
Metal nanoparticles

ABSTRACT

This mini review is limited to very recent studies (last 5–10 years) on two major issues, concerning: the production and physical/chemical modification of bacterial cellulose (BC), and its transformation into carbon and integrated synthesis of metal oxides (TiO_2, ZnO, Fe_3O_4, etc.), metal sulfide (ZnS, CdS, etc.) and metal nanoparticles (Au, Ag, Pt, Pd, etc.) within bacterial cellulose nanoribbons network. We believe that the crossover of these two domains could be of considerable interest in the view of improving the performance of materials prepared with bacterial cellulose. The diversity of these nanomaterials allows targeting of many very different properties/applications: electrochemical devices, catalysis and photocatalysis, sensors, etc. After an introduction to the most important chemical and physical characteristics of BC, production parameters, and its physical and chemical modifications, we review the use of BC as a precursor of inorganic materials like carbon and composites with metal or inorganic nanoparticles.

Contents

1. Introduction 448
2. Bacterial cellulose nanofibers 448
   2.1. History 448
   2.2. Production 448
   2.3. Structure 448
   2.4. Process parameters (temperature, C/N sources, incubation time, additives, agitation, drying) 450
   2.5. Dissolution/Suspension 453
3. Physical modifications of BC 453
4. Chemical modifications of BC 453
   4.1. Treatment with NaOH 453
   4.2. Treatment with H_2SO_4 453
   4.3. Controlled oxidation 454
   4.4. Hydrophobisation 455
   4.5. New functionalities introduced on BC 456
5. Metal oxides and sulfides from or with BC, MO-BC MS-BC 456
   5.1. Metal oxide-BC composites 456
   5.2. Metal sulfide-BC composites 458
6. Metal nanoparticles from or on bacterial cellulose, MNP-BC 458
7. Carbon from BC (CBC) and its composites with metal, metal oxide and sulfide 459

* Corresponding author.
E-mail address: bruno.boury@umontpellier.fr (B. Boury).

http://dx.doi.org/10.1016/j.carbpol.2016.09.008
0144-8617/

7.1. Only carbon 460
7.2. E-doping carbon 461
7.3. Metal nanoparticle-carbon composites 461
7.4. Metal oxide-carbon composites 462
7.5. Metal sulfide-carbon composites 462
8. Conclusion 462
Appendix A. Supplementary data 462
References 462

1. Introduction

The performances of materials are determined—from the nano- to the micro-scale—by their composition, crystallinity, morphology, porosity and hierarchical architecture. Moreover, their processing must as much as possible be in accordance with the basic principles of "Green Chemistry". In this context, bacterial cellulose has received much attention in the material science field due to some specific properties: its nanostructure, the specific balance of reactivity of the pure cellulose (from inertness to high reactivity), its compatibility with different media, its thermal stability and production from agriculture wastes.

Besides the biomedical applications that are well developed and frequently reviewed, other fields of application involving bacterial cellulose have recently emerged. Bacterial cellulose will undoubtedly become a popular material because of two important phenomena: the development and standardization of its production, and its very high performance.

In Fig. 1 there are some of these applications that are targeted by the integration of bacterial cellulose with other inorganic phases or by conversion of bacterial cellulose into carbon: metal oxide-BC (MO-BC) as photocatalyst, magnetic paper and antibacterial activity; metal sulfide-BC (MS-BC) as photocatalyst for waste treatment and water splitting; metal nanoparticles-BC (MNP-BC) as sensor, antimicrobial activities, catalyst (O_2 reduction, H_2 oxidation, waste treatment, organic reaction) and proton exchange membrane; carbon precursor (CBC) for electrochemical devices like supercapacitors and electrodes of Li- or Na-batteries. Previous reviews are interesting and connected to other issues such as electronic paper (Chen, Huang, Liang, Yao et al., 2013; Shah & Brown, 2005; Tobjörk & Österbacka, 2011).

2. Bacterial cellulose nanofibers

2.1. History

Extracellular cellulose was described by Louis Pasteur as "*a sort of moist skin, swollen, gelatinous and slippery*", and this material has long been eaten by people of the Philippines as a traditional dessert called *nata-de-coco*, i.e. 1-cm thick gel sheets fermented from coconut water. Meanwhile, the first scientific reports on this type of cellulose are "*On an acetic ferment which forms cellulose*" (Brown, 1886) and "*Further notes on the chemical action of Bacterium aceti*" (Brown, 1887) by A.J. Brown. He identified a pellicle with a chemically equivalent structure to plant cellulose, whose "growth rapidly increases until the whole surface of the liquid is covered with a gelatinous membrane, which, under very favorable circumstances, may attain a thickness of 25 mm". He concluded that "The 'vinegar plant' has no distinctive scientific name, I therefore suggest, in consideration of its power of forming cellulose, that *Bacterium xylinum* would be a suitable name for this ferment". Since that time, many reviews have summarized the advances in this domain. In the last 10 years, there have been a number of interesting reviews in relation with the main features and production of BC (Klemm et al., 2011; Moon, Martini, Nairn, Simonsen, & Youngblood, 2011; Römling & Galperin, 2015) as well as contributions revising its uses in foods (Falk, Nikita, Christian, Antje, & Thomas, 2012) composites (Shah, Ul-Islam, Khattak, & Park, 2013), drug delivery (Abeer, Mohd Amin, & Martin, 2014), wound treatment (Sulaeva, Henniges, Rosenau, & Potthast, 2015), and medical applications (Czaja, Young, Kawecki, & Brown, 2007; Lin & Dufresne, 2014). Therefore these subjects will not be considered here, see also a recent bibliometric analysis of patent publications (Charreau, Foresti, & Vazquez, 2013).

2.2. Production

Microbial cellulose is produced by various bacterial gender: *Aerobacter*, *Acetobacter*, *Achromobacter*, *Agrobacterium*, *Alacaligenes*, *Azotobacter*, *Pseudomonas*, *Rhizobium*, and *Sarcina*. Other examples are presented in Fig. 2. The advantages of bacteria producing this cellulose are still being debated: a flotation device that keeps bacteria at the oxygen-rich air/liquid interface, an anchoring device that keeps it in the rich-food source, a protection against dehydration, sunlight, and competitors, etc. At present, *Gluconacetobacter xylinus*, formerly known as *Acetobacter xylinum*, is becoming a "benchmark" since its cellulose production is sufficiently high to be of economic interest. Fig. 3 collects images of BC from *Gluconacetobacter xylinus* at different magnification.

BC is thus a biotechnology product, with production occurring mostly at the liquid/air interface, generally at $4 < pH < 7$, and $25\,^{\circ}C < T < 30\,^{\circ}C$. It is estimated that 1 bacterium can convert 108 glucose molecules per hour into cellulose. The substrate required for the production is of outmost importance; mono and polysaccharides are generally required. In recent years, research has focused on improving the use of agricultural and industrial wastes as alternative nutrients sources, with the aim of making this production "greener" and reducing production costs. There are other important issues in this field, especially regarding medium agitation and bioreactor design (Ul-Islam, Khan, Ullah, & Park, 2015).

Static cellulose production results in the formation of a gel consisting of the growth media (water and nutrients), the cellulose mat and bacteria. The next step is generally to eliminate bacteria and by-products by a NaOH treatment, followed by abundant washing with water until neutral pH. This results in a weigh loss of ±15–20%, which is ascribed to protein ±14–18% and nucleic acids ±1–1.25% (George, Ramana, Sabapathy, Jagannath, & Bawa, 2005). The jelly mass can be used in its never-dried form, or otherwise a drying step may be applied to the recovered the cellulose mat, which is an important step, with major effects on the BC structure and properties, as discussed below. Some issues now have to be tackled to allow large-scale marketing, including: high-priced substrates, low volumetric yields, upscaling difficulties and cell culture time and maintenance.

2.3. Structure

In brief, BC is pure cellulose which possesses a unique and sophisticated 3D porous network of highly crystalline (generally >80%) cellulose nanofibers with a high degree of poly-

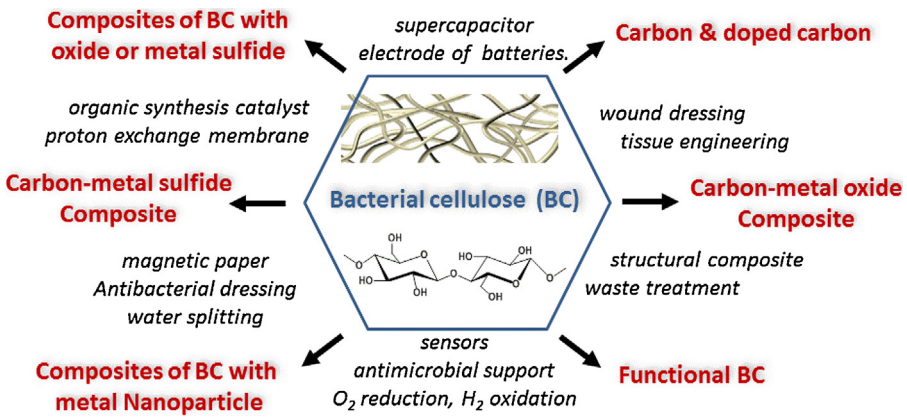

Fig. 1. General overview of chemical modifications and transformations for applications of bacterial cellulose as precursor of carbon and composites with inorganic phases.

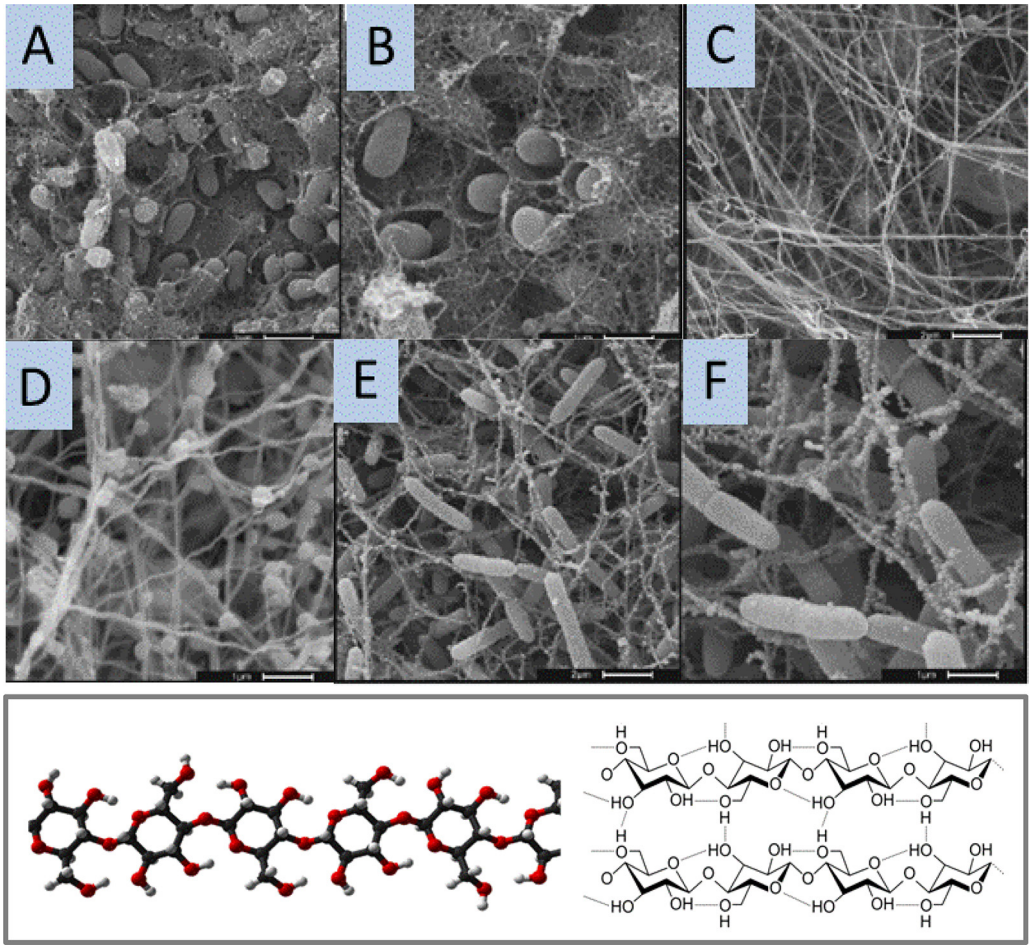

Fig. 2. SEM images of *S. enterica* ((A) and (B)), *G. xylinus* ((C) and (D)) and *D. dadantii* ((E) and (F)) biofilms, scale bars (A, C, E) 2 μm, (B, D, F) 1 μm, from Ref. (Jahn, Selimi, Barak, & Charkowski, 2011). Below is the chemical formula and structure of cellulose showing simplified H-bonding between chains.

merization (up to 8000), high water content capacity (up to 99%), high moldability, good biocompatibility, high hydrophilicity, and no toxicity. Compared to cellulose produced by plants, BC is hemicelluloses- and lignin-free. The fibers have a high aspect ratio, 20–100 nm in width and 1–9 μm length. They form a 3D network of interconnected fibers without any preferential orientation. This is the result of a biological process in which glucan chains are extruded from pores into the growth medium, where they aggregate into microfibrils.

Cellulose itself is a high molecular weight homopolymer with β-D-glucopyranose units joined by (1–4)-glycosidic links (Fig. 2). The key chemical features of this structure are: a 6-member cyclic structure with limited conformation and reactive functions like primary and secondary alcohol, and an acetal group. Carbon C1 is called the anomeric carbon and is the center of an acetal functional group. The β position is defined as the ether oxygen being on the same side of the ring as the C6 bearing the primary alcohol function. The cellulose chain ends by hemiacetal functionality on one side and a pendant hydroxyl group on the other. All of the

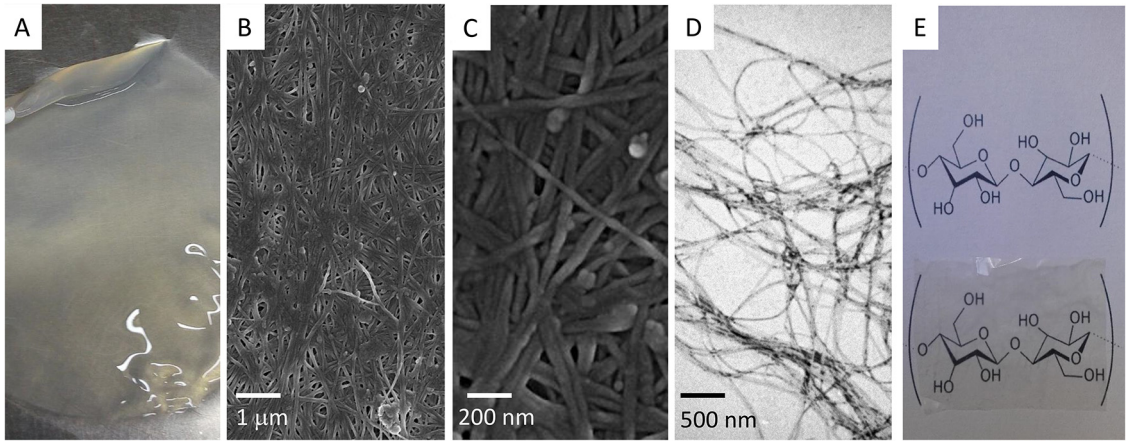

Fig. 3. Images of BC obtained with *G. xylinus* in Hestrin & Schramm medium, at 7 days under static conditions. (A) is a photograph of the produced pellicle, (B) and (C) are SEM images of dried BC pellicles, (D) is a TEM image of a diluted BC suspension obtained after 5 min homogenization in a blender, (E) illustrates the transparency of the dried BC membrane.

β-D-glucopyranose rings adopt a chair conformation, and all the hydroxyl groups are positioned in equatorial position, an important feature that allows intramolecular H-bonding between two successive rings: from O(3′)-H hydroxyl to the O(5) ring oxygen and from the O(2)-H hydroxyl to the O(6′) hydroxyl.

In BC, chains of polymer are packed essentially into cellulose Iα, cellulose Iβ and amorphous domains. The crystal structures of Iα and Iβ differ essentially by their intra-and inter-unit H-bonding network. The latter is also different for cellulose II, i.e. the most thermodynamically stable polymorph which can be produced from natural cellulose I by regeneration or mercerization. Cellulose I and cellulose II differ with respect to the conformation of the polysaccharide chain, with one being parallel and the other anti-parallel, which implies important changes in the inter- and intra-molecular H-bond network (Łaskiewicz, 1998). The consequences on the properties of the material are important for the mechanical properties, with the Young's modulus decreasing from 27 GPa (cellulose I) to 21 GPa (cellulose II) in the case of a single ramie fiber (Ishikawa, Okano, & Sugiyama, 1997).

Without any additives, ribbons produced by *Gluconacetobacter xylinus* are a mixture of Iα and Iβ, By altering the culture conditions (stirring, temperature, and additives), it is possible to alter the Iα/Iβ ratio and the microfibril width. Additives have been shown to interfere with the aggregation of elementary fibrils within the normal ribbon assembly and these modified BC microfibrils have a square cross-section and primarily have an Iβ crystal structure. Based on ^{13}C NMR and SAXS, never dried and swollen microfibrillar ribbons were described as consisting of 5 to 12 water-free Iα crystalline subunits having a cross-section of about 7 nm × 13 nm and aggregated along the (110)-lattice planes, but with each being surrounded by a layer of water. Drying does not modify the Iα/Iβ composition determined via the C-1 line in ^{13}C NMR, but microfibrillar ribbon dimensions and crystallite sizes decrease (Fink, Purz, Bohn, & Kunze, 1997). This was confirmed, as well as the fact that dehydration produces a decrease in the crystalline domain or introduces disorder (Astley, Chanliaud, Donald, & Gidley, 2001).

First SEM images of BC revealed ribbons of several hundred nanometers (Mühlethaler, 1949). They were made up of several smaller microfibrils, with the latter first being estimated to have cross-sections averaging 16Å × 58 Å (Brown, Willison, & Richardson, 1976). They were estimated by SAXS to have crystallite dimensions of ≈10Å × 60 Å, with the complete ribbon having a rectangular cross-section of ≈40Å × 500 Å^2 (Astley et al., 2001). A more recent SAXS/AFM/SEM study highlighted the presence of two populations of nanofibrils with different cross-section dimensions in BC produced by a strain of *Gluconacetobacter xylinus* in standard Hestrin–Schramm medium (see composition later on), with one being 32 nm × 16 nm and the other 21 nm × 10 nm, which differ slightly from food-grade BC obtained from commercial nata-de-coco (25 nm × 8 nm and 14 nm × 6 nm) and tunicate cellulose (25 nm × 10 nm and 15 nm × 8 nm) (Khandelwal & Windle, 2014).

In terms of thermal properties, thermal changes in the native membrane (without NaOH treatment) started at 150 °C, while membranes treated with 2N NaOH, 2N KOH, 2N K_2CO_3 or Na_2CO_3 are stable up to 275 °C, a difference that is ascribed to the residual proteins and nucleic acids in native cellulose (George et al., 2005). For treated BC, 350–355 °C is the maximum decomposition temperature (T_{max}) generally reported (see Fig. 4D) (Barud et al., 2011; George et al., 2005; George et al., 2008) and corresponding to cellulose degradation processes, such as depolymerization, dehydration, and decomposition of glycosyl units, followed by the formation of a charred residue (Oliveira et al., 2011).

2.4. Process parameters (temperature, C/N sources, incubation time, additives, agitation, drying)

Many fermentation process parameters of BC production impact the nanofiber structure and properties, especially those that can disturb the assembly of primary nanofibrils at the bacterial surface. See for example the effect of the agitation on the appearance and morphology of BC in Fig. 5A–D. The reactor temperature is also of outmost importance, while cellulose I is produced at 28 °C, the same bacteria have been reported to produce cellulose II at low temperature (4 °C) and pH 7 (Hirai, Tsuji, & Horii, 1997).

The culture medium composition also impacts on the properties of the obtained BC. In fermentation processes, macronutrients (e.g. C, O, H, N, S, P, K, Ca, Mg, Fe), micronutrients (e.g. Mn, Zn, Co, Mo, Ni, Cu) and other essential growth factors have to be provided for microorganism growth. Although at the laboratory scale the well-known Hestrin & Schramm medium (Hestrin & Schramm, 1954) (i.e. glucose (20 g L^{-1}), peptone (5 g L^{-1}), yeast extract (5 g L^{-1}), Na_2HPO_4 (2.7 g L^{-1}), citric acid (1.15 g L^{-1})) is commonly used, an important and positive evolution that must be supported is the effort in the last years to limit the use of costly raw materials of the fermentation process and to replace them by agricultural, industrial and forestry by-products and waste materials, which represent cheaper non-conventional sources of C and/or N (Carreira et al., 2011; Castro et al., 2011; Fernández Corujo, Cerrutti, Foresti, & Vazquez, 2015; Foresti, Cerrutti, & Vazquez, 2015; Rani, Rastogi et al., 2011; Vazquez, Foresti, Cerrutti, & Galvagno, 2013). Besides

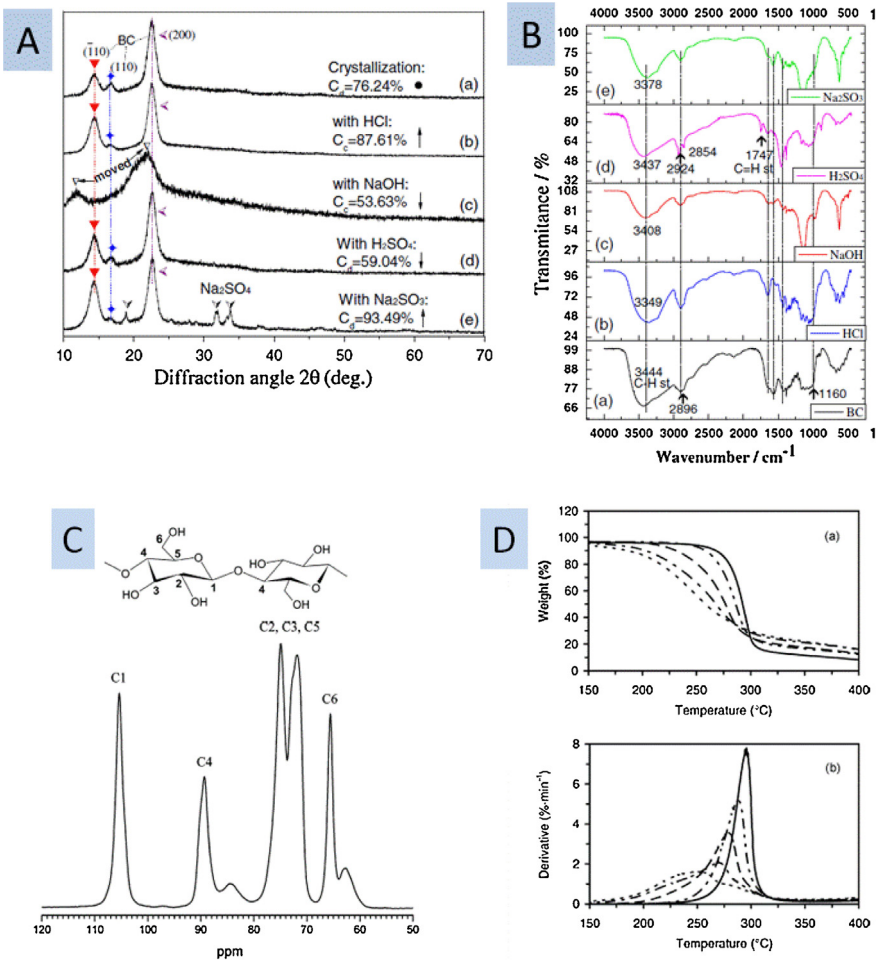

Fig. 4. Some typical analyses of BC: (A) X-ray diffraction pattern from Ref. (Wu et al., 2012); (B) FT-IR spectrum of BC from (Wu et al., 2012); (C) ^{13}C solid state NMR from Ref. (Witter et al., 2006); (D) TG and DTG curves of non-hydrolyzed pristine BC and acid hydrolyzed bacterial celluloses, from Ref. (Roman & Winter, 2004).

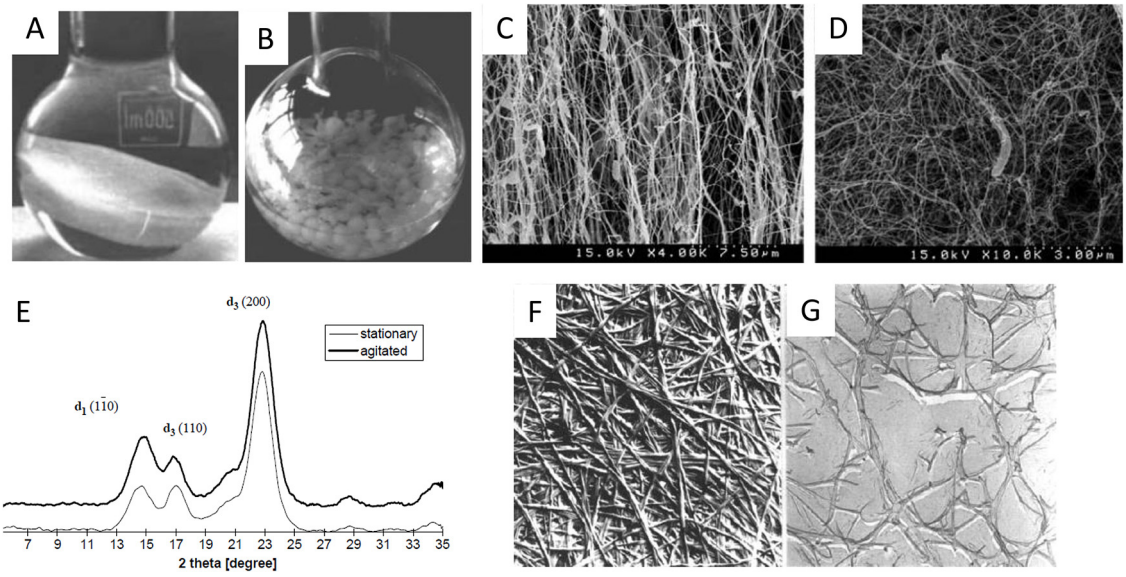

Fig. 5. Photos of (A) pellicle and (B) aggregates of BC obtained in static and agitated conditions, respectively, from Ref. (Bielecki, Krystynowicz, Turkiewicz, & Kalinowska, 2005); SEM micrographs of bacterial cellulose produced (C) statically and (D) in an agitated system; (E) X-ray diffraction patterns of bacterial cellulose produced in stationary and agitated culture conditions (from Ref. (Czaja, Romanovicz, & Brown, 2004)). Illustrations of the effect of the drying process, (F) SEM image of BC before drying and (G) after drying (from Ref. (Fink et al., 1997)).

reducing production costs, the use of waste residuals as medium for BC has an environmentally friendly effect by their removal from the environment. Together with the BC production (g/L) and/or productivity (g/L day) values achieved with the non-conventional media assayed (these values are frequently optimized by means of statistical optimization methods which consider not only the medium composition but also other process parameters such as temperature, inoculum size, surface area/volume ratio, fermentation time, etc. (Aytekin, Demirbağ, & Bayrakdar, 2016; Bilgi, Bayir, Sendemir-Urkmez, & Hames, 2016; Cerrutti et al., 2016), recent researches have frequently focused on the (BC properties/carbon source) relationship that is of major importance for its applications (Hong et al., 2012; Huang, Yang et al., 2015; Hyun, Mahanty, & Kim, 2014; Moon, Park, Chun, & Kim, 2006; Rani, Udayasankar et al., 2011; Shi et al., 2013; Suwanposri, Yukphan, Yamada, & Ochaikul, 2014; Tsouko et al., 2015). The results have generally indicated that, although the chemistry of the BC obtained is not altered, the carbon source used may have an impact on the water holding capacity (WHC) of the membranes (WHC is positively correlated with the BC porosity and surface area), their degree of polymerization, molecular weight, intrinsic viscosity, crystallinity index (67–96%), mean crystallite size (5.7–6.4 nm), water vapor transmission rate, oxygen gas transmission rate, and mechanical properties (e.g. stress at break, elongation at break, tensile strength, Young's modulus) (Hong et al., 2012; Huang, Yang et al., 2015; Hyun et al., 2014; Moon et al., 2006; Rani, Udayasankar et al., 2011; Shi et al., 2013; Suwanposri et al., 2014; Tsouko et al., 2015; Vazquez et al., 2013). On the other hand, reported changes in fibril width are really minor, mainly considering the difficulties associated with their measurement, as aggregation and twisting are very common (Hyun et al., 2014; Tsouko et al., 2015; Vazquez et al., 2013).

However, at this point it must be pointed out that many of the effects ascribed to the raw materials used in BC production with a definite bacterial strain, are actually also highly dependent on the production level achieved with each particular substrate within a certain fermentation time interval. For a specific BC harvesting time, changes in the production level achieved with each C source used highly condition the membrane density and porosity involving different levels of interaction between individual nanoribbons, which in turn have been reported to affect, for example, the membrane WHC (Tsouko et al., 2015) and tensile strength (Hong et al., 2012). In accordance with the above, for a chosen culture composition, the incubation period has also been reported to significantly affect the production and properties of the BC obtained, i.e. mainly pellicle compactness, membrane porosity, crystallinity, and average degree of polymerization (Cerrutti et al., 2016; Yang et al., 2013).

Another important trend in the production of BC is as the introduction of additives in BC fermentation medium, especially water-soluble polymers. With the aim of directly producing cellulose-polymer blends/nanocomposites, this innovative approach appears as a very interesting option that would potentially allow to reduce energy, time and chemicals consumption. Carboxymethyl cellulose, methylcellulose, hydroxypropyl methylcellulose, polyethylene oxide, polyvinyl alcohol, starch, chitosan and polyhydroxybutyrate are some examples of the polymers introduced in the BC fermentation medium (Brown & Laborie, 2007; Castro et al., 2014; Cheng, Catchmark, & Demirci, 2009; Gea, Bilotti, Reynolds, Soykeabkeaw, & Peijs, 2010; Grande et al., 2009; Huang, Chen, Lin, & Chen, 2011; Huang, Chen, Lin, Hsu, & Chen, 2010; Osorio et al., 2013; Ruka, Simon, & Dean, 2013). In many cases, it has been reported that their presence altered the structure of BC ribbons in terms of crystallinity, crystallite size, pore diameter, polymerization degree, and nanoribbon width (Cheng, Catchmark, & Demirci, 2009; Huang et al., 2011, 2010). Other additives have been found to produce major modifications in BC structure, e.g. a switch from cellulose I to cellulose II induced by a pesticide like 2,6-dichlorobenzonitrile (Yu & Atalla, 1996), or additives that increase the viscosity of the medium, or that can compete with H-bonding in the interaction of cellulose with water, like PEG (Shibazaki, Saito, Kuga, & Okano, 1998), carboxymethyl cellulose (Haigler, White, Brown, & Cooper, 1982), or xyloglucan (Hirai, Tsuji, Yamamoto, & Horii, 1998). The presence of hemicellulose (Tokoh, Takabe, Fujita, & Saiki, 1998; Uhlin, Atalla, & Thompson, 1995) or acetyl glucomannan (Tokoh et al., 1998) has another effect by modifying the Iα/Iβ ratio. On the other hand, other authors have reported on the *in situ* preparation of nanocomposites due to the incorporation of additives onto BC nanoribbons during their growth. With this approach recently nanocomposites of BC with polyvinylalcohols (Castro et al., 2014, 2015), PEO-b-PPO-b-PEO (Tercjak, Gutierrez, Barud, Domeneguetti, & Ribeiro, 2015), polycaprolactone (Figueiredo, Silvestre, Neto, & Freire, 2015), and starch (Grande et al., 2009) (among others), have been proposed. This approach seems very promising for the one-pot preparation of BC nanocomposites with better mechanical properties due to, in general, more effective component intermixing and homogenization.

Agitation is also crucial with respect to the amount of BC produced and its properties (Fig. 5A–E). In general, agitation results in increased bacterial cell growth, but decreased cellulose production compared to static conditions. The previous has been attributed to increased aeration in agitated systems, which favors cell growth and decreases the need for anchorage to the pellicle on the top of the media to obtain higher oxygen levels. However, because of the genetic instability, in agitated bioreactors some cells might convert into Cel-mutants leading to reduced BC productivity. Agitation also has an impact on the aggregation and interaction of primary fibrils with each other and with the solution. It was found that the cellulose I_α content of BC prepared in agitated cultures is lower than that of cellulose produced in static cultures (as determined by CP/MAS ^{13}C NMR), while leading to a lower Young's modulus of sheets, and a higher WHC (Watanabe, Tabuchi, Morinaga, & Yoshinaga, 1998). Although chemically identical, agitation generally lowers the crystallinity and polymerization degree of BC compared to static conditions (Algar et al., 2015; Cheng et al., 2009; Moon et al., 2006; Ruka, Simon, & Dean, 2012). Moreover, the morphology of BC produced in agitated medium is very different from that produced in static cultures. As shown in Fig. 5A and B, spherical or star-shaped pellets are obtained in agitated cultures, whereas in static fermentors bacteria produce a film or pellicle at the air-liquid medium interface.

When required, the drying process is another important parameter affecting BC properties (see SEM images of BC before and after drying in Fig. 5F and G). It can be performed essentially via three methods: room temperature at ambient pressure, freeze drying and supercritical drying (Zeng, Laromaine, Roig et al., 2014). With other nanocellulose type (i.e. nanofibrillated cellulose), supercritical drying was found to lead to the lowest thermal stability and the lowest crystallinity, with air-drying or spray-drying producing a more thermally stable material than the freeze-drying method (Peng et al., 2013). By supercritical drying using $scCO_2$, or by supercritical drying with ethanol (243 °C and 6.38 MPa), lightweight BC can reach an average density of 8.25 ± 0.7 mg cm^{-3} (40 °C and 100 bar for 2 h). Freeze-drying of 2-methyl-propan-2-ol (*ter*-butanol TBA) represents a recent and interesting advance that allows a better preservation of the porosity of cellulosic material in general and also BC (El Seoud, Fidale, Ruiz, D'Almeida, & Frollini, 2008; Fumagalli, Ouhab, Boisseau, & Heux, 2013; Sehaqui, Zhou, Ikkala, & Berglund, 2011). The mesopores diameter was about 10 nm and the surface area and pore volume about 200 m^2 g^{-1} and 0.5 cm^3 g^{-1}, respectively (Clasen, Sultanova, Wilhelms, Heisig, & Kulicke, 2006; Liebner et al., 2010). Significant crystal structure changes were reported upon drying-rehydration, especially

with an average width decrease of 4.4 nm in the (010) direction, which was more significant than that observed in the (100) and (110) directions. Rehydration led to some structural changes, but to a lesser extent. However, high temperature dehydration induced non-reversible deformation and crystal size changes, with this being ascribed to the removal of the last hydration layer on the cellulose surface (Fang & Catchmark, 2014).

2.5. Dissolution/Suspension

Development of a BC solvent is important to widen its applications and chemical modification routes. Inspired by the dissolution of other types of cellulose, NaOH was one of the earliest solvents tested. It was reported that, at 8.5% concentration at −5 °C, BC dissolution was obtained when its polymerization degree did not exceed 400. BC solubility linearly increased from 9.12 to 52.13% when [NaOH] concentration increased from 1 to 4 wt%. Urea (1–3%) was found to be efficient for drastically improving this solubility, but requires a low proportion of BC (<3%) (Łaskiewicz, 1998; Phisalaphong, Suwanmajo, & Sangtherapitikul, 2008). Other compounds that can be used are organic compounds such as *N*-methylmorpholine-*N*-oxide (NMMO) (Gao, Shen, & Lu, 2011), or metal chloride solutions like lithium chloride in *N*,*N*-dimethylacetamide (LiCl/DMAc) (Chen, Kim, Kwon, Yun, & Jin, 2009; Shen, Ji, Wang, & Yang, 2010), or aqueous solutions of zinc(II) chloride (3%) (Lu & Shen, 2011). Ionic liquids are currently being investigated, including: 1-allyl-3-methyl-imidazolium chloride (Chen, Yun, Bak, Cho, & Jin, 2010) or 1-ethyl-3-methylimidazolium acetate (Gericke, Schlufter, Liebert, Heinze, & Budtova, 2009; Okushita, Chikayama, & Kikuchi, 2012) 1-butyl-3-methylimidazolium chloride (Jinmin, Zhiyu, Xueqiong, Qinhuan, & Li, 2015; Schlufter, Schmauder, Dorn, & Heinze, 2006), 1-ethyl-3-methylimidazolium chloride (Okushita et al., 2012), 1-ethyl-3-methylimidazolium diethylphosphate (Okushita et al., 2012), or tetradecyltrihexylphosphonium bis(trifluoromethylsulfonyl)imide (Okushita et al., 2012; Tomé et al., 2011).

Such dissolution is now commonly reported, more interestingly, an investigation has recently focused on the dispersion of BC in classical organic solvents (dioxan, toluene, R-pyrrolidone,. . .), and pointed out that the closer is the liquids surface energies compared to the surface energy of BC, the higher is the concentration of exfoliated BC nanofibrils (Ferguson et al., 2016).

3. Physical modifications of BC

The BC nanofibrils structure can be changed when subjected to ultrasonic treatment. Shearing and cavitations produced by ultrasound (15–75 min 200 W, 20 kHz, 0 °C) are reported to produce nanofibril surface modifications in width, height and roughness, originating films with new nanostructures. This has impacts on the pyrolysis onset temperature (208 °C → 250–268 °C), with the crystalline material formed being type I and not type II (Tischer, Sierakowski, Westfahl, & Tischer, 2010; Wong, Kasapis, & Tan, 2009). Ultrasound treatment is also a potentially attractive tool for adaptation of the water holding capacity, viscosity and mechanical properties of BC. With a final nominal power added to each sample of 82 W, the time of the treatment is critical. Longer time (5 min) leads to an increase of the crystallinity along with entanglement of nanofibrils. A short treatment (1 min) produces break down of fibrils that are reduced to the half of the initial value (Paximada et al., 2016). BC nanofibrils can also be modified by gamma irradiation treatment. Although no significant modifications in thermal properties have been reported, a higher pore density is observed after irradiation, thus increasing the potential of these materials in drug carrier systems (Molina de Olyveira, Maria Manzine Costa, & Basmaji, 2013).

4. Chemical modifications of BC

Fig. 6 presents an overview of the main different chemical treatments that are generally reported for BC. Four main categories of reactions are, by order of importance: esterification, oxidation, silanisation and etherification. We give details of the reaction process hereafter.

4.1. Treatment with NaOH

This is a classical and old treatment of purification of BC, which is commonly treated with 2% NaOH as a standard way to kill bacteria and eliminate by-products. However, it is also well-known that at higher concentrations thermodynamically less stable cellulose I can convert into a more stable cellulose II form during mercerization through a treatment introduced by John Mercer. Many researchers have investigated the effects of key parameters (t, T, NaOH concentration) in different cellulose types (see discussion in Gea et al., 2011) and so far the debate is still open, although a 6% NaOH concentration is frequently mentioned as a condition that can produce structural changes.

On BC, NaOH and Na_2CO_3 (2N) solutions have produced conversion patterns similar to that of cellulose I into cellulose II (George et al., 2008). NaOH treatment was also reported to induce structural and morphological changes on never-dried bacterial cellulose, with an NaOH concentration above 12% that produced irregular aggregates and conversion of cellulose I into cellulose II, and both phenomena were enhanced over the treatment time. A situation different from that of cotton and that could be explained by the basic difference in microfibril organization in these materials (Shibazaki, Kuga, & Okano, 1997). Another effect reported for NaOH treatment is the possibility of chain scission, as revealed by FTIR when BC was treated with 10% NaOH at −5 °C (Wu et al., 2012).

In a recent study, native BC was treated with low concentrated aqueous NaOH (2.5%) and further purified with Na(ClO) (2.5%, r.t. overnight) (Gea et al., 2011), a well-known bleaching agent in the paper industry. In these innovative conditions, no modification in the X-ray structure has been reported, although the morphology and other characteristics (thermal stability, Young's modulus, tensile strength, elongation at break and FTIR) have revealed a purified BC. Bacterial cells are usually removed from harvested BC membranes by boiling in 2 wt% NaOH solution for 1 h, although the use of KOH (5 wt%) at room temperature overnight has also been reported (Castro et al., 2011; Vazquez et al., 2013).

4.2. Treatment with H_2SO_4

Treatments with inorganic salts and acids like sulfuric acid have been developed with the idea of enhancing the flame retardancy of BC, by promoting dehydration reactions and increasing the char yields at the expense of flammable tars. In the case of BC, with increasing concentration of the sulfate group, a significant decrease in the degradation temperature and an increase in the char fraction have been clearly observed, even at low concentration of sulfate groups (see TGA presented in Fig. 4D). For example, H_2SO_4 treatment of BC was performed in different conditions and the sulfate content was adjusted from 2.1 mmol kg^{-1} (H_2SO_4 12% w/v, 104 °C/2 h) to 73 mmol kg^{-1} (H_2SO_4 60% w/v, 60 °C/2 h), without modification of the cellulose I structure and slight amorphisation (from 85% to 72%) (Roman & Winter, 2004). H_2SO_4 treatment also produced BC fragmentation and this was developed for preparing cellulose nanocrystals (CNC) that can be micrometers in length, with a width of 5–50 nm (Hirai, Inui, Horii, & Tsuji, 2009), but this is

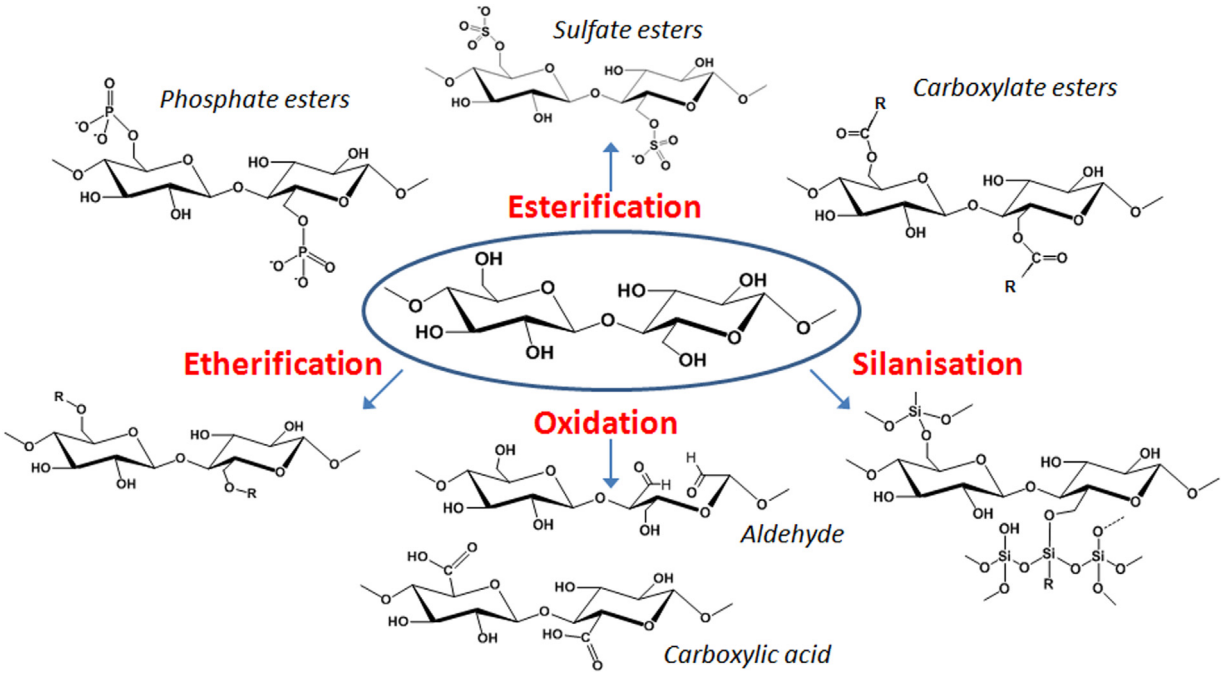

Fig. 6. General overview of the chemical modifications of BC achieved by treatment with organic and mineral reagents.

a frequently reviewed issue (Azizi Samir, Alloin, & Dufresne, 2005; de Souza Lima & Borsali, 2004; Elazzouzi-Hafraoui et al., 2008). Sulfate groups lower the thermal stability of CNC, a proposed solution consisting of their neutralization with NaOH to improve the thermal stability (Martinez-Sanz, Lopez-Rubio, & Lagaron, 2011).

A new approach consists in using SO_3/pyridine treatment of BC, but it seems of limited interest since BC is first dissolved in LiCl/DMAC at 27–50 °C for 6 h (Qin et al., 2014). The degree of sulfation ranged from 0.1 to 1.6 and could be adjusted according to the temperature and concentration. Sulfation is only regioselective C6 > C2 > C3, while leading to severe depolymerization and major modification of the crystal structure, with a cellulose II polymorphous analog being isolated (Qin et al., 2014).

4.3. Controlled oxidation

BC oxidation is done for different major applications with the aim of enhancing its biodegradability and solubility. However, the redox properties of BC represent a more important issue; with implications in other more recently investigated applications. Hence, it was reported that the BC electrochemical stability window is 0.5–5.0 V (determined by cyclovoltametry), with the material having outstanding dimensional stability (up to 180 °C). BC could thus be a good separator candidate in lithium-ion batteries (Jiang, Yin, Yu, Zhong, & Zhang, 2015), or as a scaffold for BC-carbon nanotube-ionic liquid composites for flexible supercapacitor manufacturing (Kang et al., 2012).

From the general formula of cellulose, different oxidation-reduction properties could be expected since the oxidation degree ranges from 1 to −1, to which the specificity of the end-chain terminal hemiacetal must be added.

So far, BC oxidation is essentially directed towards carboxylate (DO = III) formation from the primary alcohol on C6 (initially DO = −I), as demonstrated on other types of cellulose and nanocellulose (Coseri et al., 2013; Isogai & Kato, 1998; Isogai, Saito, & Fukuzumi, 2011). The most popular route involves 2,2,6,6-tetramethylpiperidine-1-oxyl (TEMPO) to form carboxylic groups, readily followed by FT-IR analysis (asymmetric stretching band of carboxyl groups at 1602 cm^{-1}). This oxidation has been used for the preparation of bone tissue scaffolds (Lai et al., 2015; Luo et al., 2013; Nge & Sugiyama, 2007; Park, Lee, Shin et al., 2015), Ag nanoparticles composites (Feng et al., 2014; Ifuku et al., 2007; Nge & Sugiyama, 2007), artificial muscle (Kim, Jeon, Kim, Kee, & Oh, 2015), and in composites with alginate for cell encapsulation (Park, Lee, Hyun et al., 2015).

The experimental conditions initially selected include TEMPO, NaBr, NaClO at room temperature for several hours and pH stabilized at 10.5, and is generally performed on never-dried BC (Saito, Nishiyama, Putaux, Vignon, & Isogai, 2006). Among its advantages, this process has low impact on the morphology of BC nanofibers or on its crystal structure, with some nanofiber shortening sometimes reported (Park, Lee, Hyun et al., 2015). According to ^{13}C NMR, the C6 primary hydroxyl of exposed surfaces (61.8 ppm), are the reacted ones, not the C6 primary hydroxyl inside the crystalline fibrils (64.8 ppm). The carboxylate contents can range from 0.25 mmol g^{-1} (Nge & Sugiyama, 2007) to 0.84 mmol g^{-1} (Ifuku et al., 2007; Nge & Sugiyama, 2007; Saito et al., 2006). TEMPO oxidation is currently investigated and has been combined with defibrillation (Su, Burger, Ma, Chu, & Hsiao, 2015). A recent new modification consisted of using an $NaClO_2$/Na(ClO) mixture and represent an interesting evolution since it avoids the use of NaBr (65 °C/1–30 h), leading to a carboxylate content that could be modulated from 0.2 mmol g^{-1t} to 0.95 mmol g^{-1} depending on pH and time (Lai, Zhang et al., 2013; Lai et al., 2015).

In a comparative study with periodate (see below), TEMPO was used in milder conditions (30 °C/0.5 h) to limit oxidation to aldehyde formation. Indeed, an aldehyde content as high as 0.15 mmol g^{-1} was obtained (compared to 10.02 ± 0.03 mmol g^{-1} obtained with periodate oxidation), with better BC nanofiber preservation (Luo et al., 2013).

BC is still hydrophilic after oxidation, but an increase in the contact angle with water was observed by comparison with BC, suggesting a change in the H-bonding network at the surface (Lai, Sheng et al., 2013). Another modification introduced by TEMPO is the ξ potential, which varies from −7.5 mV for BC at 6 < pH < 10 to lower values for TEMPO-BC: −39.7 (pH 4), −46.2 (pH 6) to −55.3 mV

(pH 8); TEMPO-BC fibers were unable to ionize completely at pH 4 because of the low pK_a (3,5) of carboxyl groups (Park, Lee, Shin et al., 2015).

Other oxidation processes have been investigated recently to overcome the drawback of TEMPO oxidation. Notably, BC was slowly oxidized by NO_2 at 25 °C, with [NO_2: cellulose] ± 0.2 in aphotic conditions (Peng et al., 2011; Shi et al., 2014). The oxidation progress over time preserves the crystal structure of BC and enhances its degradability *in vitro* in phosphate buffered saline solution. When NO_2-HNO_3 is used, carboxylate formation is revealed by FT-IR (1720–1760 cm^{-1}) and ^{13}C NMR (170 ppm), with a major modification also taking place at C6 (Cui et al., 2014). In this case, the extent of oxidation can be as high as 32% based on pH titration. The use of gaseous compounds, however, could limit the usefulness of this approach.

The oxidation by sodium periodate was tested to improve its biodegradability in view of its use as tissue engineering scaffolds. The reaction (40 °C/6 h/aphotic) is known to produce C2—C3 bond cleavage in the glucopyranoside ring, resulting in the formation of two aldehyde groups per glucose unit. This treatment quite well preserved the 3D-nanostructure of BC nanofibrils, but at a lower scale X-ray analyses revealed complete loss of the crystal structure and amorphisation (Li, Wan et al., 2009). Of major importance, the study shows that the biodegradation effectively started at the oxidized amorphous moieties, while allowing hydroxyapatite growth.

In terms of oxidation, it is also interesting to note that oxidative polymerization of pyrrole (Lei et al., 2016; Müller, Rambo, Recouvreux, Porto, & Barra, 2011), or aniline (Hu, Chen, Yang, Liu, & Wang, 2011) can be performed in the presence of BC, hence showing its oxidative stability toward iron(III) chloride at 25 °C or ammonium persulfate. This does not modify the morphology of BC, but some surface modifications have been reported.

4.4. Hydrophobisation

Chemical modification strategies developed to hydrophobise BC are important for its integration with organic polymers or active compounds in composites, control release or waste absorption materials, among other applications. This may be done, for example, by silanisation with Me_3SiCl (CH_2Cl_2/60 °C/4 h), without any significant modification of the crystallinity or morphology, with preservation of SS_a (160–180 $m^2\ g^{-1}$), good hydrophobisation (137.1 < contact angle < 146.5°) and a silanisation degree of 0–0.13, thus enabling fast absorption of high quantities of organic compounds such as diesel fuel waste(120 g g^{-1}) (Sai et al., 2015a). A major limitation being the limited understanding of the BC-Silane link and its extent.

Esterification (mainly acetylation) in which hydroxyl groups are partially replaced by less hydrophilic ester groups is not more a novelty for tailoring cellulose nanoparticles polarity. Following the first attempt to achieve BC acetylation (Ifuku et al., 2007; Kim, Nishiyama, & Kuga, 2002; Lee et al., 2011). Esterification lead to a substantial decrease in $\xi_{plateau}$ from −7.5 mV for BC to −22.8 mV for the modified BC that is ascribed to the hydrophobicity of the BC surface, leading to an increase in the electrolyte ion concentration in the electrochemical double layer and, therefore to a lower $\xi_{plateau}$ value (Lee et al., 2011). In general, these treatments do not alter either the morphology or the crystal structure of BC and acetylation generally occurs at C6.

Avoiding the use of solvent represents an important and positive innovation in this area. Hydrophobisation of BC has been performed in the gas phase by a solvent-free esterification process with palmitoyl chloride (170–190 °C 2–13 h) (Berlioz, Molina-Boisseau, Nishiyama, & Heux, 2009). This treatment preserved the I_α/I_β ratio of the initial BC and its basic morphology, but led to a marked weigh gain (215% for DS = 1.47), in turn leading to a marked increase in microfibril diameter (from 80 ± 20 nm to 150 ± 35 nm). BC esterification has also been conducted with anhydrides and acyl chlorides in ionic liquids, but apparently without BC fiber dissolution (Tomé et al., 2011). Indeed, the BC crystal structure, morphology and its thermal stability is mainly preserved, and the DS can range from 0.02 to 0.24. Although the esterified alcohol function has not been clearly identified, hydrophobisation is revealed by a contact angle as high as 110° when hexyl is the alkyl group of the reagent. Transparency could also be enhanced and water uptake decreased by esterification, namely acetylation (Ifuku et al., 2007). Additionally to solvent-free surface BC esterification protocols, the use of naturally occurring α-hydroxy acids as catalysts is a positive evolution (Ãvila Ramirez, Suriano, Cerrutti, & Foresti, 2014; Foresti, Avila Ramirez, Gomez, Arroyo, & Cerrutti, 2016). Table 1 in Supporting information reviews BC esterification protocols described in the literature. In most cases, the reaction conditions have been controlled in order to guarantee surface-only esterification of BC nanoribbons essentially involving OH groups on the surface or in the amorphous regions of BC, while not affecting its ultrastructure.

With a different approach, BC aerogels hydrophobisation in supercritical CO_2 with the alkyl ketene dimer (AKD) reagent has been proposed (Russler et al., 2012). AKD is a well-known sizing agent in paper production prepared from natural fatty acids and stearic acid, which is widely used to increase water repellency and thus prevent ink leaching. AKD is proposed to react with cellulose hydroxyl groups to form a β-keto ester moiety. Three different approaches for AKD modification of BC aerogels have been proposed, with the most promising route involving direct loading of aerogels with AKD dissolved in supercritical fluid, which enables an especially high degree of loading. Humidity uptake could be markedly reduced by controlling the AKD load. The use of $scCO_2$ preserved the delicate porous network structure of the aerogels without morphological changes. β-ketoesterification of bacterial cellulose with AKD at 100 °C/24 h in the presence of a small amount of 1-methylimidazole as esterification promoter has also been reported (Yoshida, Heux, & Isogai, 2012). For this innovative process that avoid the use of solvent, the reaction proceeded heterogeneously for solid cellulose in melted AKD medium. The $CHCl_3$-insoluble fraction (90% weight ratio) maintained its original morphology and had a hydrophobic nature, with DS = 1.6; whereas the $CHCl_3$-soluble fraction had a DS of 2.1.

BC dissolution in ionic liquid was reported with 1-*N*-butyl-3-methylimidazolium chloride at 80 °C/2 h with acetic anhydride and phenyl isocyanate (Schlufter et al., 2006). This was also recently explored with a modification consisting of the use of NaH as co-reagent to enhance chemical transformation. In this latter case, etherification of the alcohol function was performed in liquid ionic solution (1-butyl-3-methylimidazolium chloride) at 60 °C with NaH/CH_3-(-CH_2-)$_n$-Br (n = 1, 2, 3) as alkylating system (Jinmin et al., 2015). The alkylation DS can range from 0.21 to 2.01 depending on the experimental parameters, and in all cases the primary alcohol at C6 is the preferentially etherification one. Some of these etherified BCs are soluble in DMSO, although the crystal structure of cellulose is lost and the thermal stability is decreased, with decomposition starting at 150–200 °C.

Table 1
Some important oxido-reduction standard potentials for metal and polysaccharide.

Reagent	E_0(V)	Reaction
$(NH_4)_2[PdCl_6]$	+1.29	$PdCl_6^{2-} + 2e^- \rightarrow PdCl_4^{2-} + 2Cl^-$
	+0.62	$PdCl_4^{2-} + 2e^- \rightarrow Pd + 4Cl^-$
$(NH_4)_2[AuCl_4]$	+1.00	$AuCl_4^- + 3e^- \rightarrow Au + 4Cl^-$
Ag_2NO_3	+0.80	$Ag^+ + e^- \rightarrow Ag$
$Na_2[PtCl_6]$	+0.73	$PtCl_6^{2-} + 2e^- \rightarrow PtCl_4^{2-} + 2Cl^-$
	+0.73	$PtCl_4^{2-} + 2e^- \rightarrow Pt + 4Cl^-$
$C_6H_{12}O_6$	+0.45	$C_6H_{12}O_6 + H_2O \rightarrow C_6H_{12}O_7 + 2e^-$

4.5. New functionalities introduced on BC

New functionally is new material, but ideally chemical modification should not impact the intrinsic properties of BC. Since silanes chemistry is well-developed, silanisation of BC by functional silanes is among the very promising candidates, also if the nature of the BC-Silane link is not easy to fully characterize. Silanisation has been performed with $(EtO)_3Si-(CH_2)_3-N_3$ at RT for 18 h. After curing (105 °C/2 h), Soxhlet extraction (EtOH/18 h) and drying (105 °C/1 h), silanisation was achieved and the resulting material could then be modified by a Cu(I)-catalyzed click reaction, e.g. with acetylene-modified fluorescein (Hettegger, Sumerskii, Sortino, Potthast, & Rosenau, 2015). However, in this process, silsesquioxanes are formed by homocondensation and yields the 3D nanostructure of BC. In this type of silanisation process, genuine Si-O-cellulose linkage could be hard to achieve, ^{13}C NMR demonstrated that acidic conditions and thermal curing were the best conditions to limit homocondensation and physical adsorption (Salon et al., 2007).

Silanisation by 3-aminopropyltrimethoxysilane (APS) in acetone (25 °C/5 h; dried 110 °C/2 h) led to an N content of up to 3.4% wt and Si content 7.3% wt. Although some Si-O-cellulose can be present, homocondensation of APTS clearly occurred and led to poly-siloxanes and -silsesquioxanes polymers that covered and embedded the fine 3D architecture of BC. The material membranes showed a significant reduction in bacterial viability for both *E. coli* and *S. aureus* bacterial strains after 24 h (Fernandes et al., 2013).

Phosphatation has been performed to prepare proton-conducing membranes (Jiang, Qiao, & Hong, 2012), or metal cation absorbents (Oshima, Kondo, Ohto, Inoue, & Baba, 2008). Interesting performances have been reported in both cases, although the characterization of the modified-BC is uncompleted. BC has been treated with phytic acid, phosphoric acid (r.t., 3–6 days) (Jiang et al., 2012) or H_3PO_4 in DMF in the presence of urea (130 °C/4 h) (Oshima et al., 2008), but the effects on the crystal structure, morphology and regioselectivity were unfortunately not reported.

Recently a BC gel with phosphoric acid was reported to be dielectric, flexible and semi-transparent, and it was characterized as an electrolyte (Wang et al., 2016)

5. Metal oxides and sulfides from or with BC, MO-BC MS-BC

Cellulose has been integrated with metal oxides like demonstrated by the pioneer works of Shimizu et al. with titania (Shimizu, Imai, Hirashima, & Tsukuma, 1999) or by Dujardin et al. with silica (Dujardin, Blaseby, & Mann, 2003) with the aim of preparing a composite offering high accessibility to more or less aggregated nanoparticles of the corresponding oxide or sulfide. From this standpoint, bacterial cellulose potentially offers an isotropic 3D nano-scaffold that can perfectly host these inorganic compounds at the nanoscale. The activity of the inorganic phase is generally improved and, at least partially, ascribed to the high specific surface area of the composite resulting from the use of BC.

The simplest way to integrate BC and MO nanoparticles is to mix them under vigorous stirring. This approach can be efficient for new applications like the preparation of piezoelectric paper using $BaTiO_3$ nanoparticles (Zhang et al., 2016). Such mixing can be beneficially activated by ultrasound irradiation as reported for a ZnO-BC composite with antibacterial properties (Shahmohammadi Jebel & Almasi, 2016). Other usual preparation routes are solvo- or hydrothermal processes based on the absorption of cations by coordination to cellulose. This is no more a novelty in this area but remains interesting for new oxides. One example being ferrites like $CoFe_2O_4$-BC prepared with wet BC nanofibers in the presence of iron(III) and cobalt(II) chloride (90 °C/3 h + 90 °C/6 h), as shown in Fig. 7D–F (Menchaca-Nal et al., 2016). Upon drying, the nanofibers shrink and leave a substantial void between it and the inorganic oxides that have a nanotube-type structure, with diameters in the 120–340 nm range and having magnetic properties similar to the bulk. Finally, the direct introduction of a mineral like aTiO_2 (Dal'Acqua et al., 2015; Wesarg et al., 2012) or $CaCO_3$ (Mohammadkazemi, Faria, & Cordeiro, 2013) in the bacterial growth medium represents an innovative approach that can reduce the processing steps of the BC-metal oxide composite. As a general remark, too scarcely in these studies the chemical integrity of BC is checked, especially when temperature combined with metal salt are used. Table 2 in SI presents a list of the most recent references on the subject.

5.1. Metal oxide-BC composites

For SiO_2-BC, simple soaking of BC in a water/ethanol solution of silicon(IV) ethoxide (TEOS) and drying at 50 °C allows loading of up to 66 wt% of silica nanoparticles (Ø ± 20 nm) in the composite in which BC fibers are completely imbedded (Barud et al., 2007) A situation that is not necessary suitable depending on the targeted applications. Immersion of BC in slightly different conditions leads to SiO_2-BC composites with 30–40 wt% of silica and having a high modulus of elasticity (17 GPa at 25 °C) and tensile strength (185 Mpa) (Maeda, Nakajima, Hagiwara, Sawaguchi, & Yano, 2006; Sai et al., 2015b). Among the recent works, hydrolysis of TEOS is still the common one and was reported for the preparation of SiO_2-coated BC nanofiber of Lithium ion batteries separator (Jiang et al., 2016), or nanofibrous bioactive glass (BG) scaffold when associated with calcium (Luo et al., 2016).

For ZnO, different processes have been reported, such as a hydrothermal process at 200 °C for 2 h with zinc(II) acetate in ammonia solution (Hussein, Yahaya, Ling, & Long, 2005), a sol-gel process with hexamethylenetetramine and zinc(II) nitrate at 90 °C for 60 min (Costa, Goncalves, Zaguete, Mazon, & Nogueira, 2013), and a solvothermal process with zinc(II) acetate in diethylene glycol at 170–180 °C (see Fig. 7A and B) (Chen, Zhou et al., 2013), or a two-step process (78 °C/5 h) followed by autoclaving in ethanol and hexamine (85 °C/6 h) (Wang, Schutz et al., 2014; Wang, Zhao et al., 2014). The particle size can range from 20 to >500 nm and loading can be adapted according to the BC/ZnO-precursor ratio. Even under harsher conditions, the BC structure does not seem to be modified, as assessed by FTIR or X-ray diffraction. Recently, wet and Zn^{2+}-satured BC was used in solution plasma process disclosed for the preparation of ZnO-BC (1.44 kV, a pulse frequency 15 Hz, a pulse width 2.0 μs, gap distance of 1 mm), and different morphology of ZnO was obtained when compared to classical route (Janpetch, Saito, & Rujiravanit, 2016).

For TiO_2, the goal is generally to increase the specific surface and hence the catalytic activity; very different materials can be prepared. For example, in a first attempt, TiO_2 nanowires were obtained after sol-gel processing of BC with a TiO_2 precursor ($Ti(O^nBu)_4$), followed by calcination at 500 °C (Zhang & Qi, 2005). In that case, BC was only a sacrificial template and, for the resulting TiO_2 pure oxide, the BET-specific surface area and pore volume being respectively 61 $m^2\,g^{-1}$ and 0.20 $cm^3\,g^{-1}$. In another approach, TiO_2-BC composites were obtained by solvothermal processing at 200 °C in ethanol (see Fig. 7C) (Sun, Yang, Wang et al., 2010). This material exhibited a nanofibril structure with BC fibers being completely covered by the oxide and 30 nm <Ø < 50 nm, here the BET SSa was 220 $m^2\,g^{-1}$ and the pore volume was 0.15 $cm^3\,g^{-1}$. However, BC seemed to be relatively modified, as revealed by X-ray analysis, although FTIR analysis findings indicated its presence. For this material, the photocatalytic activity was slightly better than that of P25 (Evonik), certainly due to the high specific surface area and small nanocrystal size. The use of such TiO_2-BC composite to

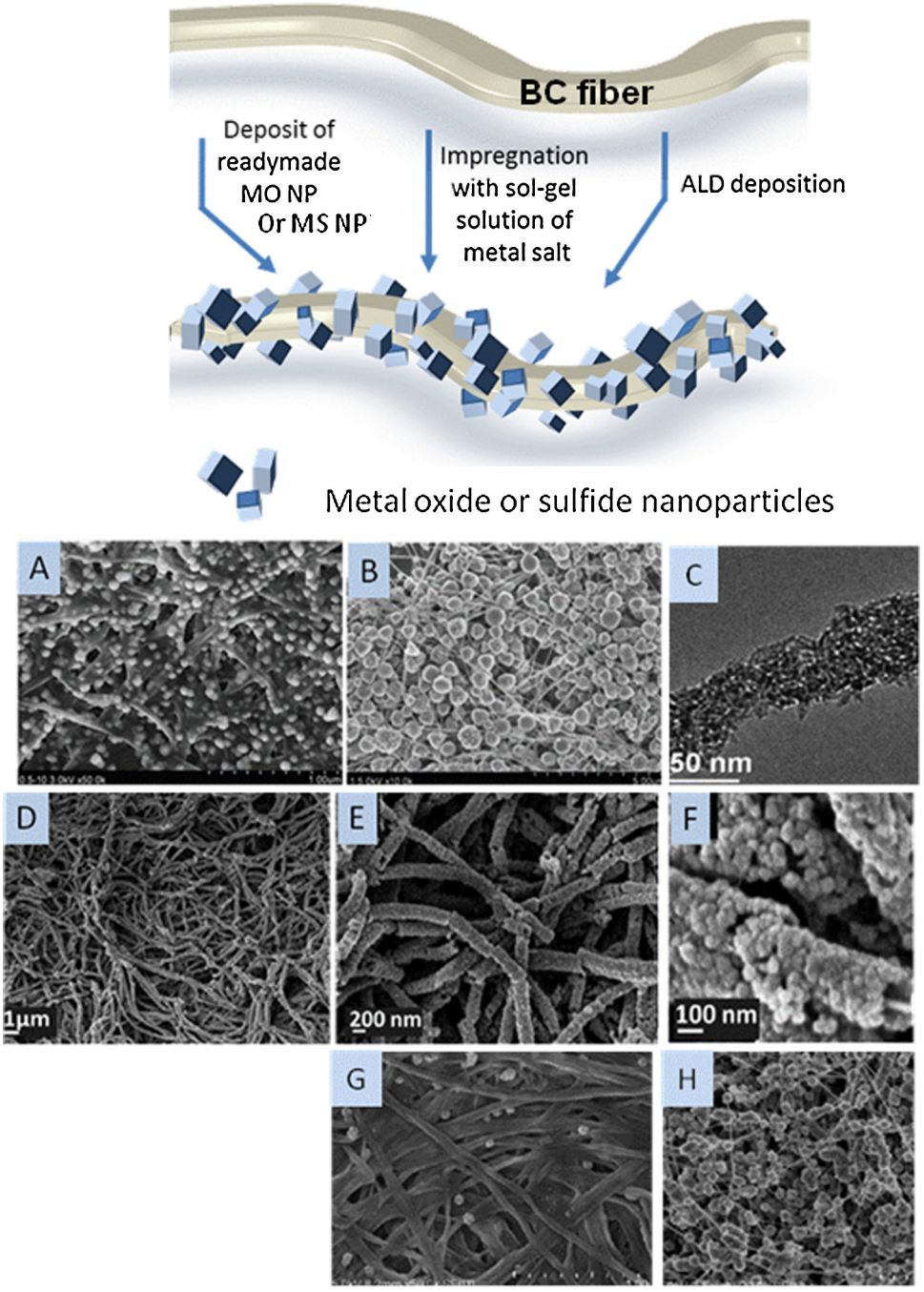

Fig. 7. Schematic representation of a MONP-BC or a MSNP-BC nanocomposite and the different routes to prepare it. (A) and (B) are SEM images of ZnO-BC synthesized at different concentrations of zinc acetate: (A) 0.5 wt% and (B) 5 wt% in diethylene glycol at 170–180 °C from Ref. (Chen, Zhou et al., 2013); (C) is a TEM image of TiO_2-BC hybrid nanofibers by solvothermal at 200 °C in ethanol from Ref. (Sun, Yang, Wang et al., 2010); and (D), (E) and (F) are SEM images of $CoFe_2O_4$-CB composite at different magnifications, from Ref. (Menchaca-Nal et al., 2016). (G) and (H) are SEM images of ZnS-BC nanocomposites synthesized at different zinc precursor concentrations: (G) 0.5 wt%, and (H) 5 wt%, from Ref. (Zheng et al., 2014).

enrich and detect phosphorylated proteins represents an innovative and attractive application (Gao et al., 2016).

For iron oxide, besides the simple precipitation from the metal salt (Stoica-Guzun et al., 2016), synthesis has been carried out in solvothermal conditions with BC, iron(III) nitrate and urea in aqueous solution autoclaved for 48 h at 120 °C, leading to an Fe_2O_3-BC composite (Wan, Yang, Xiong, Guo et al., 2015; Wan, Yang, Xiong, Luo et al., 2015). At this step, the process did not seem to modify the BC crystal structure. Subsequently, this composite could be converted into an Fe_3O_4-C composite by pyrolysis at 600 °C with a high F_3O_4 content (30–60 wt%), high BET SS_a (322 $m^2\,g^{-1}$) and exhibit interesting electrochemical properties as an anode for LIB (reversible capacity of the binder-free electrodes being 754 mA h g^{-1} at 100 mA g^{-1} after 100 cycles). Similar solvothermal reactions with 1,6-hexanediamine/iron(III) chloride/BC in ethylene glycol (200 °C/6 h) led to a Fe_3O_4-BC composite whose nanoparticles formed on the surface of nanofibrils are much smaller than in the absence of BC, and they covered the fibers or were well dispersed along them (Nata, Sureshkumar, & Lee, 2011). This material had among the highest absorption capacities for As(V) 36.5 mg g^{-1} of such F_3O_4-cellulose composites developed for those applications.

Another Fe_3O_4-BC was prepared using iron(II) and iron(III) chloride in basic aqueous solution and PEG under ultrasound irradiation. Magnetite nanoparticles of <100 nm size are found to cover BC fibers, with the crystallite size being around 10–15 nm according to X-ray analysis. The use of PEG and ultrasound clearly improved the nanoparticles dispersion (Zheng et al., 2013). Microwave activation, an innovation for such processes, was used with iron(III) acetylacetonate to treat BC that was previously dried in different conditions: room-temperature drying, freeze-drying, and supercritical-drying (Zeng, Laromaine, Feng et al., 2014). The treatment is short and carried out at 200 °C with Fe_3O_4 loading adjusted from 4 to 40% as a function of the type of drying used for BC preparation. This is another example of the high impact of the processing of BC before its use in the preparation of materials.

5.2. Metal sulfide-BC composites

For these types of composites, the preparation can simply involve solution processing at room temperature, or be more sophisticated and involve a solvothermal process. A list of the most recent references is given in Table 3 in SI. Importantly, most of them do not seem to modify the BC structure, which is generally checked by X-ray and SEM. Thus, CdS-BC preparation was reported to be as simple as contact of CB with aqueous solution of a Cd(II) salt followed by contact with aqueous sodium sulfide (Li, Chen et al., 2009; Li, Wan et al., 2009). In these conditions, CdS nanoparticles (Ø 30 nm) are dispersed along the fibers, a very positive point for applications and that justifies the use of BC. A solvothermal process (ethanol/water) can also be used (Yang et al., 2011), and gives CdS nanoparticles that are well dispersed along the fibers, with the size being around 30 nm for 3 h of reaction. This particle size increases with the reaction time, e.g. Ø ± 50 nm after 7 h of reaction. The same authors reported the formation of CdSe-BC nanocomposites with luminescent properties (Yang et al., 2012).

For ZnS-BC, a simple method involves a BC solution treatment with thioacetamide at 80 °C for 3 h without apparent modification of BC nanofibers. Nanoparticles of 9 < Ø < 17 nm can be either dispersed along the nanofibers or completely aggregated and entirely covering the BC, with this being essentially a question of concentration/amount of reactants (0.1–5 wt%), as shown in Fig. 7G and H (Zheng, Chen, Zhao, Zheng, & Wang, 2014). Ion exchange is an original approach developed for the $Zn_xCd_{1-x}S$-BC composite and based on solvothermal treatment of ZnO-BC with thiourea and different proportions of cadmium(II) chloride at 120 °C for 6 h. Zinc oxide is transformed into ZnS simultaneously to the formation of CdS, with both reactions leading to nanoparticles of 5 < Ø < 5–8 nm either aggregated or completely covering the initial BC fibers (Wang, Geng et al., 2015; Wang, Hou et al., 2015; Wang, Sun et al., 2015).

In terms of application, the photocatalytic activity of CdS-BC for the degradation of methyl orange in UV (<420 nm) appears to be higher than that of the benchmark P25 (Evonik), and especially much more efficient than that of CdS alone. A clear demonstration of the advantages of the BC nano-scaffold is that it allows higher accessibility and reactivity (Yang et al., 2011). For ZnS-BC, fluorescent material at 468 nm under UV (330–385 nm) was observed at low ZnS concentration (1 wt%) and might be used for detection/sensors. The blue-shift observed compared to that of the bulk ZnS material (485 nm) was about 17 nm (Zheng et al., 2014), so $Zn_xCd_{1-x}S$-BC composites were tested as visible-light photocatalytic agents for water splitting with visible light ($\lambda \geq 420$ nm) in an aqueous solution of Na_2S and Na_2SO_3 as sacrificial reagents. $Zn_{0.09}Cd_{0.91}S$/BC exhibits highest H_2 evolution rate: 1450 $\mu mol\, h^{-1}\, g^{-1}$, 15 times that of the commercial CdS powder (96 $\mu mol\, h^{-1}\, g^{-1}$).

6. Metal nanoparticles from or on bacterial cellulose, MNP-BC

In Fig. 8 the different ways to prepare a nanocomposite MNP-BC are schematized. However, mixing ready-made particles is always possible due to the chemical properties of BC. Two additional routes allow *in situ* generation of MNP, either by taking advantage of the chemical stability of BC toward the reducing agent, or by using the reducer property of BC toward of a metal salt. This latter case represents a more innovative route relying on the reducing and coordinating BC behavior, as shown by other types of cellulose that lead to metal salt reduction and the formation of Pt (Johnson, Thielemans, & Walsh, 2011), Ag (Mochochoko, Oluwafemi, Jumbam, & Songca, 2013), or Au (in ionic liquids) (Li, Friedrich, & Taubert, 2008) nanoparticles. Complexation of the initial metal cation by cellulose is a very important point to succeed in this approach, and several studies have been carried out on this phenomenon, see for example the case of Cu(II) by cellulose of lyocells (Emam, Manian, Široká, & Bechtold, 2012; Emam et al., 2014). The reaction temperature is of major importance (25–800 °C), leading to either metal oxide persistence, or metal nanoparticles formation or metal carbide formation (Hoekstra, Versluijs-Helder, Vlietstra, Geus, & Jenneskens, 2014). For other metals like Mn, the controlled reduction of potassium permanganate by carboxymethyl cellulose allows the formation of suboxides like Mn_3O_4 and MnO_2, oxohydroxide MnO(OH) and carbonate $MnCO_3$ (Yin, Gao, Wu, Wang, & Lu, 2010). A list of the most recent references on this subject is given in Table 4 in SI.

Silver and gold are the easiest metal nanoparticles that can obtained by *in situ* oxidation of BC by Ag(I) and Au(III) salt at 60–100 °C in aqueous solution. In similar conditions, Pd-NMP can be produced by the reduction of $(NH_4)_2(PdCl_6)$, but under the same conditions, Pt-MNP are not obtained from hexachloroplatinate(VI), a more kinetically inert complex with higher thermal stability (Cotton & Wilkinson, 1988), see also recent work on BC assemblies with Pt (Aritonang, Onggo, Ciptati, & Radiman, 2015; Huang et al., 2014; Mi et al., 2016), and Ag nanoparticles, (Pourreza, Golmohammadi, Naghdi, & Yousefi, 2015; Rieger, Cho, Yeung, Fan, & Schiffman, 2016).

The electrochemical potential (E_0(V)) in Table 1 below suggests that the reducing ends of cellulose fibrils can effectively produce this reduction. In these reactions, BC behaves specifically. It was noticed that cotton linters do not produce the same MNP formation. The difference was explained by the much looser structure of BC, which offers access to reducing (aldehyde) end groups in bacterial cellulose (Evans, O'Neill, Malyvanh, Lee, & Woodward, 2003). Particles of 5–30 nm are well dispersed in the BC nano-architecture and strongly linked to it. Generally, but not always, the crystal structure and crystallinity of BC are not modified by the treatment, but this point must be closely checked. Using Tollen's reagent $[Ag(NH_3)_2]^+$, evidence of cellulose oxidation, especially at the C6 and the formation of carboxylic groups is provided by FTIR spectroscopy, with some of these carboxylic groups being additional coordinating groups (Zhang, Zheng, Liu et al., 2015).

For these *in situ* generated MNP-BC composites, the advantageous effect of BC was highlighted in many different applications. As an optical sensor whose detection efficiency is based on the plasmonic properties of MNP, the latter were found to be well dispersed throughout the BC paper, and the composite was found to be efficient for the detection of organic compounds that modify MNP by oxidizing or aggregating them. While the porosity and reactivity of BC is the key to preparing MNP, its transparency is crucial for the sensing properties (Morales-Narvez et al., 2015). With Ag, similar MNP-BC have antibacterial properties against *E. coli*, *S. aureus* as well as *P. aeruginosa*, and the low toxicity being explained by the slow Ag^+ release, which means they could be used as biocompatible

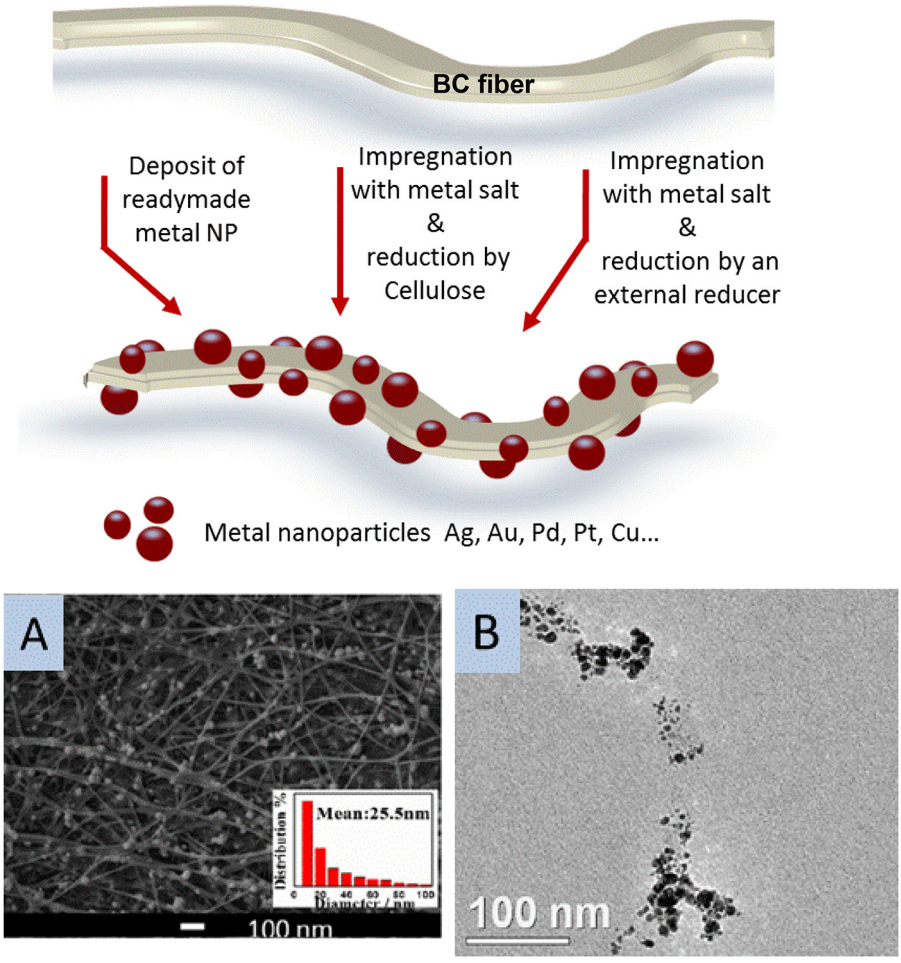

Fig. 8. Schematic representation of a MNP-BC nanocomposite and different routes to prepare it. (A) is a SEM image of AgNP-BC nanocomposite prepared by in situ generation of Ag NP from Ref. (Zhang, Zheng, Liu et al., 2015), (B) is a TEM image of Pd-Cu-BCF nanocomposite using $NaBH_4$ as reducer from Ref. (Sun, Yang, Li et al., 2010).

antimicrobial wound dressing (see SEM images in Fig. 8A) (Zhang, Zheng, Liu et al., 2015). In the electrochemical domain, although BC has no activity the corresponding AgNP-CB composite shows high electrocatalytic activity toward the oxygen reduction reaction ascribed to the small diameter of silver nanoparticles that are well dispersed in the BC network (Zhang, Zheng, Liu et al., 2015). PdNP-BC catalyzed hydrogen generation, and the thermal stability for application in fuel and biofuel cells is better than NAFION (Evans et al., 2003).The reduction of metal nitrate by cellulose has now be extended to other metal nanoparticles like Fe, Co & Ni, and represents a new route for Metal-C nanocomposites (Ma et al., 2016).

For metals that cannot be produced upon reduction by BC, the old strategy is to add a reducing agent. Different ones may be used thanks to the chemical stability of BC: Na(BH_4) or HCHO (Yang et al., 2009), K(BH_4) (Sun, Yang, Li et al., 2010) and poly(ethylenimine) (Zhang et al., 2010), while ultrasound activation was reported as a new and innovative way to increase the Ag-NP loading quantity (Zhijiang, Chengwei, Guang, & Jaehwan, 2012).

Metal particles frequently have Ø < 10 nm and are dispersed along the fibers or can completely cover their surface, depending on the experimental conditions (T, t, and concentration), as clearly shown with Pt NP prepared by reduction with poly(ethylenimine) (Zhang et al., 2010). In the same study, it was shown that the presence of halide and its interaction in forming halide-metal bonds can disturb the MNP-BC interaction, as exemplified by the case of Au. Copper, as nanoparticles and nanowires, has been combiTned with BC, but with an external reducing agent like $NaBH_4$ or $NaBH_4$/hydrazine (Pinto, Neves, Neto, & Trindade, 2012; Shao et al., 2016), Ni nanoparticles is another recent example {Thiruvengadam, 2016 #1373). For such "copper paper", it was found that BC had an inhibitory effect on the oxidation of Cu NPs which was higher than that of plant cellulose, a phenomenon that could be explained by the open 3D-structure of BC. Magnetron sputtering deposition of metal nanoparticles is a new process used in this field for the preparation of such "copper paper" (Lv et al., 2016).

In terms of application, PtNP-BC had thermal stability at around 250 °C and high electrocatalytic activity in hydrogen oxidation reactions for application in fuel cells (Yang et al., 2009). PtCuNP-CB has good catalytic activity for the reduction of nitrate into nitrogen via formic acid (see TEM image of the material in Fig. 8B) (Sun, Yang, Li et al., 2010). Horseradish peroxidase enzymes can be integrated into Au–BC nanocomposites to produce an amperometry biosensor of H_2O_2 that can be detected at concentrations as low as 1 μM (Zhang et al., 2010), or glucose as low as 2.3 μM (Wang et al., 2010). In the case of PdNP-BC composites, high catalytic activity and good recyclability have been reported for Heck coupling reactions and Suzuki coupling reactions in water (Zhou et al., 2012a,b).

7. Carbon from BC (CBC) and its composites with metal, metal oxide and sulfide

Cellulose conversion into carbonaceous materials was probably first done soon after humans mastered fire. Such carbonaceous

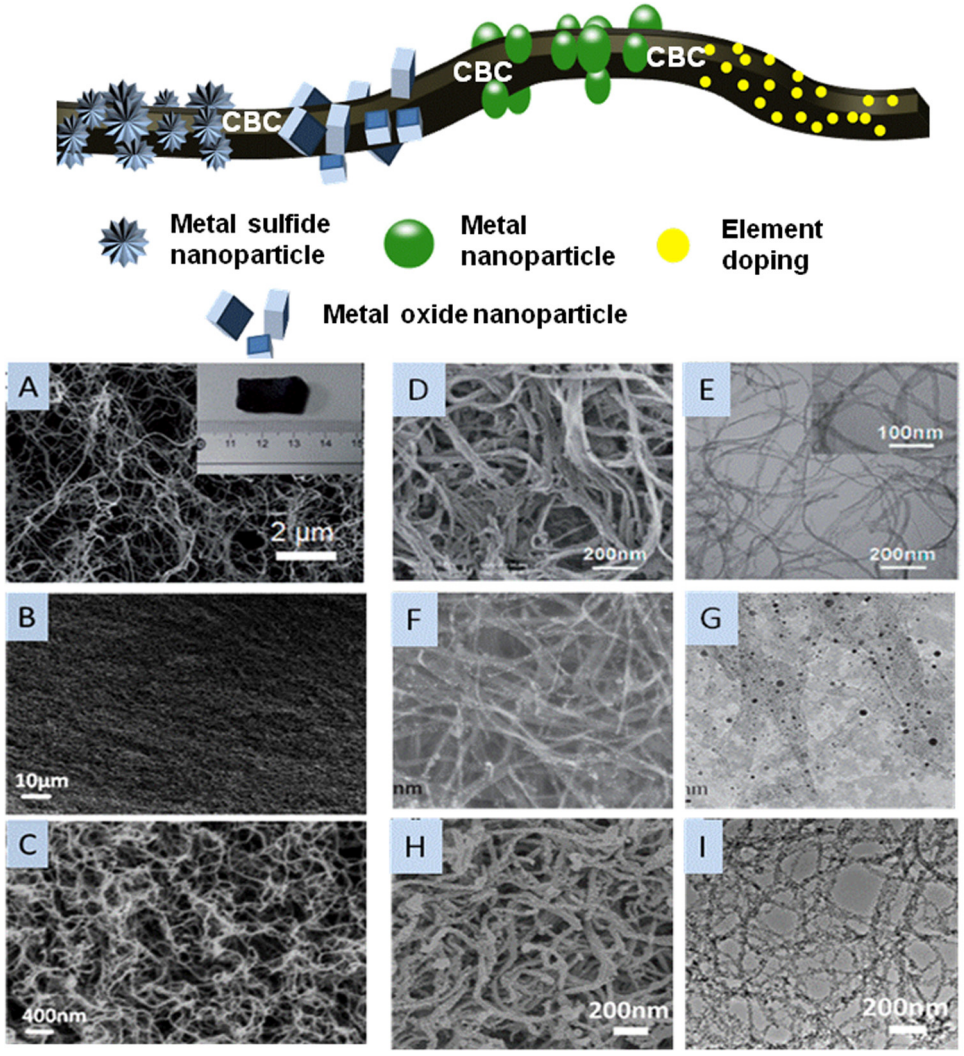

Fig. 9. Schematic representation of a CBC forming nanocomposite either with metal sulfide, metal oxide or metal NP and the case of an element-doped CBC. (A) is a SEM and an optical image of CBC aerogel treated at 1300 °C from Ref. (Wu et al., 2013); (B) and (C) are SEM micrographs at different magnification of CBC prepared at 900 °C aerogels from Ref. (Wang, Schutz et al., 2014). Respectively SEM (D) and TEM (E) images of an N-doped CBC, from Ref. (Chen, Huang, Liang, Yao et al., 2013). Respectively SEM (F) and TEM (G) images of an Ru-CBC nanocomposite from Ref. (Tong et al., 2015). Respectively SEM (H) and TEM (I) images of a SnO_2-BC nanocomposite from Ref. (Wang, Li et al., 2013; Wang, Yu et al., 2013).

materials must now fulfill requirements for catalysis, waste treatment and energy applications. Additionally, a prerequisite is to achieve C-nanomaterials at a large scale and low cost by sustainable and fully standardized methods. Following pioneer work on carbon aerogels, BC appears to be a prime candidate to fulfill all of the above-mentioned prerequisites (Pekala, Alviso, & LeMay, 1990). But as is the case for other materials, the C nano-architecture is not paramount, the polymorph is another key. Disordered carbons have attracted attention due to high electrical conductivity, offering a large inter layer space that favors Li^+ or Na^+ insertion and extraction. Such carbons can be obtained by pyrolysis of biopolymers like gelatin and magnesium citrate (Guan et al., 2015), glucose (Tang et al., 2012), chitosan (Wang, Hou et al., 2015; Wu et al., 2015), and starch (Falco et al., 2011; Wang, Yu et al., 2013; Wilamowska, Graczyk-Zajac, & Riedel, 2013). Below we discuss the different carbonaceous materials that can be prepared from BC and that are schematically illustrated in Fig. 9. If BC is an interesting candidate in this field, a precise and comprehensive comparison between different cellulosic materials, i.e. plant-derived nanofibrillated cellulose, bacterial cellulose nanoribbons, cellulose nanocrystals and filter paper, still remains to be done and reported.

7.1. Only carbon

Although the simplest one, the carbon production via pyrolysis of bacterial cellulose (CBC) has been developed with the idea that the size and crystallinity of the 3D network could result in slightly different properties (Hiroyoshi, Shigeru, Masaru, & Katsumi, 2002). Pyrolysis of BC up to 2000 °C allows the formation of graphitic carbon and highlights the key role of the BC drying process prior to pyrolysis. In the best cases, a modest specific surface area of 60–120 $m^2\,g^{-1}$ is obtained (Kuga, Kim, Nishiyama, & Brown, 2002). In an investigation on the potentiality of CBC-hydroxyapatite composites as biomaterials for bone tissue engineering, the thermal decomposition and structural patterns of BC nanofibers showed that graphitization of BC started at 600 °C and had a typical graphitic structure at 3200 °C (Wan et al., 2011).

Pyrolysis at 700–1300 °C of freeze-dried BC aerogels under argon led to CBC aerogels with a marked decrease in the density, i.e. 9–10 $mg\,cm^{-3}$ for BC → 4–6 $mg\,cm^{-3}$ for CBC, and in the diameter, i.e. 20–80 nm for BC → 10–20 nm for CBC. The innovative point is that this CBC had other interesting properties: flexibility, flame stability, high conductivity of 20.6 $S\,m^{-1}$ and its hydrophobic character makes it efficient for organic pollutant adsorption

(see material in Fig. 9A) (Wu, Li, Liang, Chen, & Yu, 2013; Wu, Liang, Chen, Hu, & Yu, 2016). In recent studies, CBC nanofibers of about 20 nm, with a surface area of 670 $m^2 g^{-1}$ and a pore volume of 0.83 $cm^3 g^{-1}$, were reported for BC pyrolyzed at 900 °C. Essentially amorphous CBC is characterized at low temperature (900 °C), with graphitization being improved by increasing the temperature or by the presence of Fe nanoparticles introduced prior to pyrolysis (see in Fig. 9B and C) (Wang, Schutz et al., 2014). This material was found to have interesting features as anodes in LIBs: charge–discharge curves at a current density of 75 mA g^{-1}, namely 0.2 C (1C = 372 mA g^{-1}). The initial discharge and charge capacities were 797 mA h g^{-1} and 386 mA h g^{-1}, respectively, while the initial charge capacity of 386 mA h g^{-1} decreased to 359 mA h g^{-1} after 100 cycles.

When blended with graphene oxide and pyrolyzed, the CBC composites have electrical conductivity of up to 171 S m^{-1}. Importantly, a mass-specific capacitance of 160 F g^{-1} at a 0.4 A g^{-1} current density and a capacitance retention of 90.3% after 2000 cycles were demonstrated for the composite electrode in supercapacitor applications (Liu, Zhou et al., 2015).

To improve the CBC performance, as for other types of carbon, treatment involving simple contact with KOH prior a second pyrolysis at 700 °C/1 h led to a marked increase in the specific surface area (497 $m^2 g^{-1} \rightarrow$ 1235 $m^2 g^{-1}$). Moreover, the electrochemical performances are improved, including the specific capacity of over 857.6 mAh g^{-1} after 100 cycles at 100 mA g^{-1} while retaining a high capacity of 325.38 mAh g^{-1} even when cycled at a high current density of 4000 mA g^{-1} (Wang, Sun et al., 2015). Similarly, pyrolysis of a freeze-dried composite obtained by immersing BC into KOH solution (0.05, 0.10, 0.20 and 0.50 M) has led to carbons with original morphology and good supercapacitors properties. This being ascribed to the effect of KOH in promoting inter-crosslinking and polycondensation of BC fibers, acting as a hard template and etching carbon atoms during the carbonization process (Shan, Yang, Liu, Yan, & Fan, 2016).

Urea, a chemical frequently associated with cellulose chemistry, was employed in an original way in the pyrolysis of a BC/urea mixture at 900 °C, leading to a complex structure consisting of carbon nanofibers and graphene sheets. At an intermediate temperature of 600 °C, carbon nitride was found to be produced by thermal reaction of BC and urea. With a high SSA (782 $m^2 g^{-1}$) and a robust porous 3D structure, both electron and mass transfer were found to be favored, resulting in high electrochemical performances and stability as catalyst for the oxygen reduction reaction in alkaline media (Ye, Lv, Li, Xu, & Chen, 2014).

In a completely different approach, bacterial cellulose was introduced in a usual solvothermal process of production of carbonaceous spheres from glucose. After immersion of BC in a 0.5 M glucose solution and treatment at 180 °C for 3 or 6 h, a remarkable material made of carbonaceous spheres and BC fibers exhibited high performances Pb(II) and Fe(III) absorption, respectively, for 200 mg and 1134 mg gm^{-1} of carbonaceous pellicles. It was noted that BC apparently limited growth of the carbonaceous sphere to around 0.1–1 mm, which was bigger than when prepared without BC. However, surprisingly, the fate of BC in these conditions was not documented (Nata & Lee, 2010).

Well established by previous studies, high temperature solvothermal biopolymer processing can produce different types of functional carbons (Hu et al., 2010). Based on this background, poorly graphitized carbon with SSa ±200 $m^2 g^{-1}$ and a total pore volume of 0.15 $cm^3 g^{-1}$ were produced by hydrothermal treatment (200 °C/8 h). (Liu, Jiang et al., 2015; Liu, Zhou et al., 2015).

For such CBCs the adsorption of Sr(II) and Cs(I) as chemical analogues of ^{90}Sr and ^{137}Cs was reported recently. The absorption capacity according to a Langmuir model at pH 4.5 and 293 K is respectively 67.11 mg g^{-1} and 57.47 mg g^{-1}, and presents a potential interest for nuclear waste treatments (Sun et al., 2016).

7.2. E-doping carbon

Doping with heteroatoms, such as N or B is now recognized as a way to improve some of the properties of carbon. For example, the capacity performance for the carbon-based anode for LIBs can be enhanced by N-doping inducing additional active sites to absorb Li^+. Three routes are known at present, the basic one for E-doping (E = N, P or B) of CBC involves pre-impregnation of BC by aqueous solution of salts such as H_3PO_4, $NH_4H_2PO_4$ and H_3BO_3/H_3PO_4, followed by pyrolysis at 800 °C (Chen, Huang, Liang, Gao, & Yu, 2014). Having a high specific surface area (280–510 $m^2 g^{-1}$) these N,P-doped CBCs exhibited the best specific supercapacitance of all the ones tested, which could be increased at 1.0 A g^{-1} from 129.19 to 204.9 F g^{-1} by increasing the $[(NH_4)H_2PO_4]$ used for pre-impregnation from 0.02 to 0.1 mol L^{-1}. These N,P-doped CBC retained an energy density of 1.86 Wh kg^{-1}, with a high power density of 26.61 kW kg^{-1} at a current density of 100 A g^{-1}. Like in many other cases, the results are attractive, but the understanding of the pyrolysis chemistry is not very accessible.

Another old and simple way for E-doping is to pyrolyse in N-rich reactive atmosphere as known for many other ceramics. Such material was obtained with N content = 5.8% and SS_a = 916 $m^2 g^{-1}$ by treatment of CBC in an NH_3 atmosphere at 700–900 °C (Liang, Wu, Chen, Li, & Yu, 2015). These materials were successfully tested as electrode material for electrochemical reduction of oxygen and as cathode catalysts for constructing air electrodes of Zn-air batteries. N-CBC have voltages of 1.34 and 1.25 V at discharge current densities of 1.0 and 10 mA cm^{-2}, respectively.

More recent is the introduction of N by BC-blending with polypyrrole as a N-provider precursor. BC-polypyrrole blend can been prepared by oxidative polymerization of pyrrole in wet BC pellicle (Müller et al., 2011). The pyrolysis of such blends leads to N-doped carbon depending on the BC/polypyrrole ratio and experimental parameters (Chen, Huang, Liang, Yao et al., 2013). Recently reported, a supercapacitor with N-doped BC has a reversible specific capacity of 240 mAh g^{-1} at 100 mA g^{-1} over 100 cycles, rate performance of 146.5 mAh g^{-1} at 1000 mA g^{-1}, and cycling stability of 148.8 mAh g^{-1} at 500 mA g^{-1} over 400 cycles (Zhang, Zhang, Zhao et al., 2015).

For S-doping, a post-treatment of CBC by solvothermal treatment 160 °C/12 h can be carried out with a S/CS_2 solution. Tested for Li-S batteries, this S-doped CBC shows a discharge capacity of 1134 mA h g_{Sul}^{-1} at 200 mA g^{-1} and a long-term cycle stability of 700 mA h g_{Sul}^{-1} at 400 mA g^{-1} over 400 cycles, with a good rate capability (Huang, Zheng et al., 2015). In another approach, targeting N-doped CBC, treatment of CBC up to 800 °C under argon-CO_2 mixture was followed by solvothermal treatment (180 °C/12 h) in aqueous ammonia. Although the chemistry is poorly understood, the N-doped flexible CBC device exhibited a maximum power density of 390.53 kW kg^{-1} and a long life span, with ~95.9% of the initial specific capacitance after 5000 cycles (see SEM and TEM images of the material in Fig. 9D and E) (Chen, Huang, Liang, Yao et al., 2013).

7.3. Metal nanoparticle-carbon composites

Mixing with metal nanoparticles is a third route for improvement of the electrochemical properties of CBC, like ruthenium nanoparticles that were prepared by contact of CBC with a Ru(II) chloride solution followed by pyrolysis (1000 °C/1 h/H_2/Ar) and had good performances for material of cathode for Li–O_2 batteries (see TEM and SEM images of the material in Fig. 9F and G). The recharge potential was around 3.97 V at 1000 mA h g^{-1}. Furthermore, the

discharge–recharge curves remained almost identical after 25 continuous cycles, with a capacity cut-off of 500 mA h g_{total}^{-1} at 200 mA g^{-1}. Ru-CBC showed good activity and stability for round-trip cycles, which could be attributed to the adaptability for Li_2O_2 deposition and transport of oxygen and electrons. (Tong et al., 2015). Ge-loaded CBCs were tested as anodes of LiBs and prepared with $GeBr_2$, oleylamine and CBC by a solvothermal process (260 °C/12 h) (Wang, Li et al., 2013; Wang, Yu et al., 2013). For this Ge-loaded material after 100 cycles at a current rate of 100 mA g^{-1}, the specific capacity remained a high value of around 500 mAh g^{-1}, with a reasonable rate capability with a stable capacity of around 230 mAh g^{-1} under fast (700 mA g^{-1}) discharge/charge cycling.

7.4. Metal oxide-carbon composites

Metal oxide nanoparticles are generally formed by pyrolysis of an MO-BC composite, see for example the recent $CoFe_2O_4$-CBC preparation as efficient electro catalyst for oxygen reduction and evolution (Liu, Yan, Cao, Zhou, & Yang, 2016). Another approach is to first prepared a CBC aerogel that is then impregnated with metal oxide precursors like in the case of Fe_2O_3-CBC as anode for lithium ion batteries (Huang et al., 2016). SnO_2-loaded CBC was prepared by a CBC and $SnCl_2$ solvothermal process (150 °C/15 h/H_2O-$C_2O_2H_6$), see SEM and TEM images in Fig. 9H and I (Wang, Li et al., 2013; Wang, Yu et al., 2013). For this material, the following properties were reported: a reversible capacity of around 600 mAh g^{-1} after 100 cycles under a current density of 100 mA g^{-1} with a specific capacity of around 380 mAh g^{-1} under a very high current density of 1 A g^{-1} could be obtained on the basis of the total electrode weight. Here again, the performances, compared to bare SnO_2, is ascribed to the well-dispersed nanoparticles, the interwelded carbon nanofibrils structure and numerous interconnected voids facilitating the diffusion of lithium ions.

Reported for preparing materials for supercapacitor applications, MnO_2-CBC was prepared by deposition of MnO_2 using the redox reaction with MnO_4^- and C from CBC (Chen, Huang, Liang, Guan et al., 2013). The equation below accounts for this transformation:

$$4K^+ + 4MnO_4^- + 3C + H_2O \rightarrow 4MnO_2 + CO_3^{2-} + 2HCO_3^- + 4K^+$$

With MnO_2-CBC as positive electrode and N-doped CBC as a negative electrode, the optimized supercapacitor can be reversibly charged/discharged at 2.0 V (in 1.0 M Na_2SO_4), reaching an energy density of 32.91 W h kg^{-1}, a power density of 284.63 kW kg^{-1}, with 95.4% specific capacitance retained after 2000 cycles.

7.5. Metal sulfide-carbon composites

For other applications, e.g. catalysts for electrochemical production of H_2, CBC was assembled with MoS_2 nanoparticles by a two-step process (Guo et al., 2015). CBC obtained by pyrolysis at 900 °C of CB was reacted with $(NH_4)_2MoS_4$ and hydrazine (200 °C/10 h) in DMF. The flexible MoS_2/CNF foam exhibited catalytic activity for a hydrogen evolution reaction (HER) in acidic electrolytes (16 mA cm^{-2} at an overpotential of 230 mV) and showed an over-potential of 120 mV, a Tafel slope of 44 mV dec^{-1}, an exchange current density of 0.09 mA cm^{-2}, and a Faradic efficiency of nearly 100%.

By a similar route and for similar applications, pyrolysis of BC-aniline mixture led to N-supplemented CBC that could then be hybridized with MoS_2 by a hydrothermal process with $(NH_4)_6(Mo_7O_{24})\cdot 4H_2O$. The electrocatalytic activity for HER was characterized by an overpotential of 108 mV, high current density of 8.7 mA cm^{-2} at $\eta = 200$ mV, low Tafel slope of 61 mV dec^{-1}, and even excellent stability. The nano-architecture provided by N-doped CBC and its electronic conductivity were the two main reasons for such performances (Lai, Miao, Huang, Zhang, & Liu, 2016). An alternative of the preparation of such MoS_2-C is a hydrothermal process of ammonium molybdate with thiourea (200 °C for 24 h) followed by pyrolysis. Is has excellent performance as anode for lithium-ion batteries (specific discharge capacities up to 1140 mA h g^{-1} at the C-rate of 1C) (Li et al., 2016).

Ni_3S_2-CBC composites were prepared for supercapacitor application. Starting with BC pyrolyzed at 800 °C, the formation of separated nanoparticles Ni_3S_2 ($10 < Ø < 30$) at the surface of CBC was obtained by hydrothermal processing with $NiCl_2\cdot 6H_2O$, CN_2H_4S and ammonia at 180 °C for 12 h. In an asymmetric supercapacitor with Ni_3S_2/CBC and CBC as positive and negative electrodes, respectively, the following electrochemical performances were obtained: operating potential up to 1.7 V, specific capacitance of 68.8 F g^{-1} at 5 mV s^{-1}, the energy density of 25.8 Wh kg^{-1} at a power density of 425 W kg^{-1} and cycle life with only a 3% drop-off after 2500 cycles.

8. Conclusion

Bacterial cellulose is certainly a key material for innovation and high-tech applications of the future. Particularly, this overview revealed that, besides composite reinforcement and biomedical applications of BC which have been receiving much attention in the last decade, there is another very promising field of application of BC in which its well-defined structure is highly suitable for the preparation of inorganic materials assembled with BC, or produced by its decomposition. Important advances in this field will be the development of greener processes for association/transformation of BC into mineral active phase. Besides, standardization of the experiments, at least to some extent would lead to more rationalization and understanding.

However, for this and any other application of BC at large scale, higher BC production yield, reduced incubation duration and lower production costs, are still required in order to meet industry needs. A review of recent contributions on BC production evidences the efforts that are currently being done in this direction, including the continuous search for agro-industrial wastes/by-products to be used as low-cost suitable carbon sources, the optimization of culture conditions, the search for BC-producing strains with enhanced productivity, and the design of new cultivation systems.

Finally, although it is possible to produce BC with diverse morphologies, porosities, water holding capacities, etc; and different surface modifications of BC can be carried out; how BC characteristics influence its transformation, and at the end the properties of the BC-inorganic materials produced, remain issues to be more systematically investigated.

Appendix A. Supplementary data

Supplementary data associated with this article can be found, in the online version, at http://dx.doi.org/10.1016/j.carbpol.2016.09.008.

References

Ãvila Ramirez, J. A., Suriano, C. J., Cerrutti, P., & Foresti, M. L. (2014). Surface esterification of cellulose nanofibers by a simple organocatalytic methodology. *Carbohydrate Polymers*, *114*, 416–423.

Abeer, M. M., Mohd Amin, M. C. I., & Martin, C. (2014). A review of bacterial cellulose-based drug delivery systems: Their biochemistry, current approaches and future prospects. *Journal of Pharmacy and Pharmacology*, *66*(8), 1047–1061.

Algar, I., Fernandes, S. C. M., Mondragon, G., Castro, C., Garcia-Astrain, C., Gabilondo, N., et al. (2015). Pineapple agroindustrial residues for the production of high value bacterial cellulose with different morphologies. *Journal of Applied Polymer Science*, *132*(1). January 5

Aritonang, H. F., Onggo, D., & Ciptati Radiman, C. L. (2015). Insertion of platinum particles in bacterial cellulose membranes from PtCl4 and H2PtCl6 precursors. *Macromolecular Symposia*, *353*(1), 55–61.

Astley, O. M., Chanliaud, E., Donald, A. M., & Gidley, M. J. (2001). Structure of Acetobacter cellulose composites in the hydrated state. *International Journal of Biological Macromolecules*, *29*(3), 193–202.

Aytekin, A., Demirbağ, D. D., & Bayrakdar, T. (2016). The statistical optimization of bacterial cellulose production via semi-continuous operation mode. *Journal of Industrial and Engineering Chemistry*, *37*, 243–250.

Azizi Samir, M. A. S., Alloin, F., & Dufresne, A. (2005). Review of recent research into cellulosic whiskers, their properties and their application in nanocomposite field. *Biomacromolecules*, *6*(2), 612–626.

Barud, H. S., Assunção, R. M. N., Martines, M. A. U., Dexpert-Ghys, J., Marques, R. F. C., Messaddeq, Y., et al. (2007). Bacterial cellulose–silica organic–inorganic hybrids. *Journal of Sol-Gel Science and Technology*, *46*(3), 363–367.

Barud, H., Ribeiro, C., Capela, J., Crespi, M., Ribeiro, S., & Messadeq, Y. (2011). Kinetic parameters for thermal decomposition of microcrystalline, vegetal, and bacterial cellulose. *Journal of Thermal Analysis & Calorimetry*, *105*(2), 421–426.

Berlioz, S., Molina-Boisseau, S., Nishiyama, Y., & Heux, L. (2009). Gas-phase surface esterification of cellulose microfibrils and whiskers. *Biomacromolecules*, *10*(8), 2144–2151.

Bielecki, S., Krystynowicz, A., Turkiewicz, M., & Kalinowska, H. (2005). Bacterial cellulose. In *Biopolymers online*. Wiley-VCH Verlag GmbH & Co. KGaA.

Bilgi, E., Bayir, E., Sendemir-Urkmez, A., & Hames, E. E. (2016). Optimization of bacterial cellulose production by Gluconacetobacter xylinus using carob and haricot bean. *International Journal of Biological Macromolecules*, *90*, 2–10.

Brown, E. E., & Laborie, M.-P. G. (2007). Bioengineering bacterial cellulose/poly(ethylene oxide) nanocomposites. *Biomacromolecules*, *8*(10), 3074–3081.

Brown, J. R. M., Willison, J. H. M., & Richardson, C. L. (1976). Cellulose biosynthesis in Acetobacter xylinum: Visualization of the site of synthesis and direct measurement of the in vivo process. *Proceedings of the National Academy of Sciences of the United States of America*, *73*, 4564–4569.

Brown, A. J. (1886). XLIII. -On an acetic ferment which forms cellulose. *Journal of the Chemical Society Transactions*, *49*(0), 432–439.

Brown, A. J. (1887). LXII. -Further notes on the chemical action of Bacterium aceti. *Journal of the Chemical Society Transactions*, *51*(0), 638–643.

Carreira, P., Mendes, J. A. S., Trovatti, E., Serafim, L. S., Freire, C. S. R., Silvestre, A. J. D., et al. (2011). Utilization of residues from agro-forest industries in the production of high value bacterial cellulose. *Bioresource Technology*, *102*(15), 7354–7360.

Castro, C., Zuluaga, R., Putaux, J.-L., Caro, G., Mondragon, I., & Ganan, P. (2011). Structural characterization of bacterial cellulose produced by Gluconacetobacter swingsii sp. from Colombian agroindustrial wastes. *Carbohydrate Polymers*, *84*(1), 96–102.

Castro, C., Vesterinen, A., Zuluaga, R., Caro, G., Filpponen, I., Rojas, O. J., et al. (2014). In situ production of nanocomposites of poly(vinyl alcohol) and cellulose nanofibrils from Gluconacetobacter bacteria: Effect of chemical crosslinking. *Cellulose*, *21*(3), 1745–1756.

Castro, C., Zuluaga, R., Rojas, O. J., Filpponen, I., Orelma, H., Londono, M., et al. (2015). Highly percolated poly(vinyl alcohol) and bacterial nanocellulose synthesized in situ by physical-crosslinking: Exploiting polymer synergies for biomedical nanocomposites. *RSC Advances*, *5*(110), 90742–90749.

Cerrutti, P., Roldán, P., García, R. M., Galvagno, M. A., Vázquez, A., & Foresti, M. L. (2016). Production of bacterial nanocellulose from wine industry residues: Importance of fermentation time on pellicle characteristics. *Journal of Applied Polymer Science*, *133*(14), n/a–n/a.

Charreau, H., Foresti, M. L., & Vazquez, A. (2013). Nanocellulose patents trends: A comprehensive review on patents on cellulose nanocrystals, microfibrillated and bacterial cellulose. *Recent Patents on Nanotechnology*, *7*(1), 56–80.

Chen, P., Kim, H.-S., Kwon, S.-M., Yun, Y. S., & Jin, H.-J. (2009). Regenerated bacterial cellulose/multi-walled carbon nanotubes composite fibers prepared by wet-spinning. *Current Applied Physics*, *9*(suppl. (2)), e96–e99.

Chen, P., Yun, Y. S., Bak, H., Cho, S. Y., & Jin, H.-J. (2010). Multiwalled carbon nanotubes-embedded electrospun bacterial cellulose nanofibers. *Molecular Crystals and Liquid Crystals*, *519*(1), 169–178.

Chen, L.-F., Huang, Z.-H., Liang, H.-W., Gao, H.-L., & Yu, S.-H. (2014). Three-Dimensional heteroatom-doped carbon nanofiber networks derived from bacterial cellulose for supercapacitors. *Advanced Functional Materials*, *24*(32), 5104–5111.

Chen, L.-F., Huang, Z.-H., Liang, H.-W., Guan, Q.-F., & Yu, S.-H. (2013). Bacterial-cellulose-derived carbon nanofiber@MnO2 and nitrogen-doped carbon nanofiber electrode materials: An asymmetric supercapacitor with high energy and power density. *Advanced Materials*, *25*(34), 4746–4752.

Chen, L.-F., Huang, Z.-H., Liang, H.-W., Yao, W.-T., Yu, Z.-Y., & Yu, S.-H. (2013). Flexible all-solid-state high-power supercapacitor fabricated with nitrogen-doped carbon nanofiber electrode material derived from bacterial cellulose. *Energy & Environmental Science*, *6*(11), 3331–3338.

Chen, S., Zhou, B., Hu, W., Zhang, W., Yin, N., & Wang, H. (2013). Polyol mediated synthesis of ZnO nanoparticles templated by bacterial cellulose. *Carbohydrate Polymers*, *92*(2), 1953–1959.

Cheng, K.-C., Catchmark, J. M., & Demirci, A. (2009). Effect of different additives on bacterial cellulose production by Acetobacter xylinum and analysis of material property. *Cellulose*, *16*(6), 1033–1045.

Clasen, C., Sultanova, B., Wilhelms, T., Heisig, P., & Kulicke, W. M. (2006). Effects of different drying processes on the material properties of bacterial cellulose membranes. *Macromolecular Symposia*, *244*(1), 48–58.

Coseri, S., Biliuta, G., Simionescu, B. C., Stana-Kleinschek, K., Ribitsch, V., & Harabagiu, V. (2013). Oxidized cellulose: Survey of the most recent achievements. *Carbohydrate Polymers*, *93*(1), 207–215.

Costa, S. V., Goncalves, A. S., Zaguete, M. A., Mazon, T., & Nogueira, A. F. (2013). ZnO nanostructures directly grown on paper and bacterial cellulose substrates without any surface modification layer. *Chemical Communications*, *49*(73), 8096–8098.

Cotton, F. A., & Wilkinson, G. (1988). *Advanced inorganic chemistry*. New York: Wiley.

Cui, Q., Zheng, Y., Lin, Q., Song, W., Qiao, K., & Liu, S. (2014). Selective oxidation of bacterial cellulose by NO2-HNO3. *RSC Advances*, *4*(4), 1630–1639.

Czaja, W., Romanovicz, D., & Brown, R. M. (2004). Structural investigations of microbial cellulose produced in stationary and agitated culture. *Cellulose*, *11*(3), 403–411.

Czaja, W. K., Young, D. J., Kawecki, M., & Brown, R. M. (2007). The future prospects of microbial cellulose in biomedical applications. *Biomacromolecules*, *8*(1), 1–12.

Dal'Acqua, N., Mattos d, A. B., Krindges, I., Pereira, M. B., Barud d, H. S., Ribeiro, S. J. L., et al. (2015). Characterization and application of nanostructured films containing Au and TiO2 nanoparticles supported in bacterial cellulose. *The Journal of Physical Chemistry C*, *199*, 340–349.

de Souza Lima, M. M., & Borsali, R. (2004). Rodlike cellulose microcrystals: Structure, properties, and applications. *Macromolecular Rapid Communications*, *25*(7), 771–787.

Dujardin, E., Blaseby, M., & Mann, S. (2003). Synthesis of mesoporous silica by sol-gel mineralisation of cellulose nanorod nematic suspensions. *Journal of Materials Chemistry*, *13*(4), 696–699.

El Seoud, O. A., Fidale, L. C., Ruiz, N., D'Almeida, M. L. O., & Frollini, E. (2008). Cellulose swelling by protic solvents: Which properties of the biopolymer and the solvent matter? *Cellulose*, *15*(3), 371–392.

Elazzouzi-Hafraoui, S., Nishiyama, Y., Putaux, J.-L., Heux, L., d. r, D. F., & Rochas, C. (2008). The shape and size distribution of crystalline nanoparticles prepared by acid hydrolysis of native cellulose. *Biomacromolecules*, *9*(1), 57–65.

Emam, H. E., Manian, A. P., Široká, B., & Bechtold, T. (2012). Copper inclusion in cellulose using sodium D-gluconate complexes. *Carbohydrate Polymers*, *90*(3), 1345–1352.

Emam, H. E., Manian, A. P., Široká, B., Duelli, H., Merschak, P., Redl, B., et al. (2014). Copper(I)oxide surface modified cellulose fibers: Synthesis, characterization and antimicrobial properties. *Surface and Coatings Technology*, *254*, 344–351.

Evans, B. R., O'Neill, H. M., Malyvanh, V. P., Lee, I., & Woodward, J. (2003). Palladium-bacterial cellulose membranes for fuel cells. *Biosensors and Bioelectronics*, *18*(7), 917–923.

Falco, C., Perez Caballero, F., Babonneau, F., Gervais, C., Laurent, G., Titirici, M.-M., et al. (2011). Hydrothermal carbon from biomass: Structural differences between hydrothermal and pyrolyzed carbons via 13C solid state NMR. *Langmuir*, *27*(23), 14460–14471.

Falk, L., Nikita, A., Christian, S., Antje, P., & Thomas, R. (2012). Bacterial cellulose aerogels: From lightweight dietary food to functional materials. functional materials from renewable sources. *American Chemical Society*, 57–74.

Fang, L., & Catchmark, J. (2014). Structure characterization of native cellulose during dehydration and rehydration. *Cellulose*, *21*(6), 3951–3963.

Feng, J., Shi, Q., Li, W., Shu, X., Chen, A., Xie, X., et al. (2014). Antimicrobial activity of silver nanoparticles in situ growth on TEMPO-mediated oxidized bacterial cellulose. *Cellulose*, *21*(6), 4557–4567.

Ferguson, A., Khan, U., Walsh, M., Lee, K.-Y., Bismarck, A., Shaffer, M. S. P., et al. (2016). Understanding the dispersion and assembly of bacterial cellulose in organic solvents. *Biomacromolecules*, *17*(5), 1845–1853.

Fernandes, S. C. M., Sadocco, P., Alonso-Varona, A., Palomares, T., Eceiza, A., Silvestre, A. J. D., et al. (2013). Bioinspired antimicrobial and biocompatible bacterial cellulose membranes obtained by surface functionalization with aminoalkyl groups. *ACS Applied Materials & Interfaces*, *5*(8), 3290–3297.

Fernández Corujo, V., Cerrutti, P., Foresti, M. L., & Vazquez, A. (2015). Production of bacterial cellulose from non conventional low cost fermentation media. In D. Puglia, E. Fortunati, & J. Kenny (Eds.), *Multifunctional polymeric nanocomposites based on cellulosic nanoreinforcements*. Tsouko: Elsevier.

Figueiredo, A. R. P., Silvestre, A. J. D., Neto, C. P., & Freire, C. S. R. (2015). In situ synthesis of bacterial cellulose/polycaprolactone blends for hot pressing nanocomposite films production. *Carbohydrate Polymers*, *132*, 400–408.

Fink, H.-P., Purz, H. J., Bohn, A., & Kunze, J. (1997). Investigation of the supramolecular structure of never dried bacterial cellulose. *Macromolecular Symposia*, *120*(1), 207–217.

Foresti, M. L., Cerrutti, P., & Vazquez, A. (2015). Bacterial nanocellulose: Synthesis, properties and applications. In *Polymer nanocomposites based on inorganic and organic nanomaterials*. pp. 39–61. John Wiley & Sons, Inc.

Foresti, M. L., Avila Ramirez, J. A. A., Gomez, H., Catalina Arroyo, S., & Cerrutti, P. (2016). Naturally occurring α-Hydroxy acids: Useful organocatalysts for the acetylation of cellulose nanofibres. *Current Organocatalysis*, *2*, 1–8.

Fumagalli, M., Ouhab, D., Boisseau, S. M., & Heux, L. (2013). Versatile gas-phase reactions for surface to bulk esterification of cellulose microfibrils aerogels. *Biomacromolecules*, *14*(9), 3246–3255.

Gao, Q., Shen, X., & Lu, X. (2011). Regenerated bacterial cellulose fibers prepared by the NMMO·H2O process. *Carbohydrate Polymers*, *83*(3), 1253–1256.

Gao, R., Chen, X., Chen, C., Shi, R., Ouyang, F., Yang, J., et al. (2016). Synthesis of BC@mTiO2 hybrid nanofibers for highly efficient enrichment and detection of phosphopeptides. *Cellulose*, *23*(4), 2475–2485.

Gea, S., Bilotti, E., Reynolds, C. T., Soykeabkeaw, N., & Peijs, T. (2010). Bacterial cellulose-poly(vinyl alcohol) nanocomposites prepared by an in-situ process. *Materials Letters*, *64*(8), 901–904.

Gea, S., Reynolds, C. T., Roohpour, N., Wirjosentono, B., Soykeabkaew, N., Bilotti, E., et al. (2011). Investigation into the structural, morphological, mechanical and thermal behaviour of bacterial cellulose after a two-step purification process. *Bioresource Technology*, *102*(19), 9105–9110.

George, J., Ramana, K. V., Sabapathy, S. N., Jagannath, J. H., & Bawa, A. S. (2005). Characterization of chemically treated bacterial (Acetobacter xylinum) biopolymer: Some thermo-mechanical properties. *International Journal of Biological Macromolecules*, *37*(4), 189–194.

George, J., Sajeevkumar, V. A., Kumar, R., Ramana, K. V., Sabapathy, S. N., & Bawa, A. S. (2008). Enhancement of thermal stability associated with the chemical treatment of bacterial (Gluconacetobacter xylinus) cellulose. *Journal of Applied Polymer Science*, *108*(3), 1845–1851.

Gericke, M., Schlufter, K., Liebert, T., Heinze, T., & Budtova, T. (2009). Rheological properties of cellulose/ionic liquid solutions: From dilute to concentrated states. *Biomacromolecules*, *10*(5), 1188–1194.

Grande, C. J., Torres, F. G., Gomez, C. M., Troncoso, O. P., Canet-Ferrer, J., & Martínez-Pastor, J. (2009). Development of self-assembled bacterial celluloseâ€starch nanocomposites. *Materials Science and Engineering: C*, *29*(4), 1098–1104.

Guan, Z., Liu, H., Xu, B., Hao, X., Wang, Z., & Chen, L. (2015). Gelatin-pyrolyzed mesoporous carbon as a high-performance sodium-storage material. *Journal of Materials Chemistry A*, *3*(15), 7849–7854.

Guo, X., Cao, G.-, Ding, F., Li, X., Zhen, S., Xue, Y.-, et al. (2015). A bulky and flexible electrocatalyst for efficient hydrogen evolution based on the growth of MoS2 nanoparticles on carbon nanofiber foam. *Journal of Materials Chemistry A*, *3*(9), 5041–5046.

Haigler, C. H., White, A. R., Brown, R. M., & Cooper, K. M. (1982). Alteration of in vivo cellulose ribbon assembly by carboxymethylcellulose and other cellulose derivatives. *The Journal of Cell Biology*, *94*(1), 64–69.

Hestrin, S., & Schramm, M. (1954). Synthesis of cellulose by Acetobacter xylinum. 2. Preparation of freeze-dried cells capable of polymerizing glucose to cellulose. *Biochemical Journal*, *58*(2), 345–352.

Hettegger, H., Sumerskii, I., Sortino, S., Potthast, A., & Rosenau, T. (2015). Silane meets click chemistry: Towards the functionalization of wet bacterial cellulose sheets. *ChemSusChem*, *8*(4), 680–687.

Hirai, A., Tsuji, M., & Horii, F. (1997). Culture conditions producing structure entities composed of Cellulose I and II in bacterial cellulose. *Cellulose*, *4*(3), 239–245.

Hirai, A., Tsuji, M., Yamamoto, H., & Horii, F. (1998). In situ crystallization of bacterial cellulose III. Influences of different polymeric additives on the formation of microfibrils as revealed by transmission electron microscopy. *Cellulose*, *5*(3), 201–213.

Hirai, A., Inui, O., Horii, F., & Tsuji, M. (2009). Phase separation behavior in aqueous suspensions of bacterial cellulose nanocrystals prepared by sulfuric acid treatment. *Langmuir*, *25*(1), 497–502.

Hiroyoshi, T., Shigeru, Y., Masaru, I., & Katsumi, Y. (2002). Anode performance of pyrolyzed bacterial cellulose in secondary lithium-ion batteries and the effect of added metal phthalocyanines. *Japanese Journal of Applied Physics*, *41*(5R), 3137.

Hoekstra, J., Versluijs-Helder, M., Vlietstra, E. J., Geus, J. W., & Jenneskens, L. W. (2014). Carbon-supported base metal nanoparticles: Cellulose at work. *ChemSusChem*, *8*(6), 985–989.

Hong, F., Guo, X., Zhang, S., Han S.-f. Yang, G., & Jönsson, L. J. (2012). Bacterial cellulose production from cotton-based waste textiles: Enzymatic saccharification enhanced by ionic liquid pretreatment. *Bioresource Technology*, *104*, 503–508.

Hu, B., Wang, K., Wu, L., Yu, S.-H., Antonietti, M., & Titirici, M.-M. (2010). Engineering carbon materials from the hydrothermal carbonization process of biomass. *Advanced Materials*, *22*(7), 813–828.

Hu, W., Chen, S., Yang, Z., Liu, L., & Wang, H. (2011). Flexible electrically conductive nanocomposite membrane based on bacterial cellulose and polyaniline. *The Journal of Physical Chemistry B*, *115*(26), 8453–8457.

Huang, H.-C., Chen, L.-C., Lin, S.-B., Hsu, C.-P., & Chen, H.-H. (2010). In situ modification of bacterial cellulose network structure by adding interfering substances during fermentation. *Bioresource Technology*, *101*(15), 6084–6091.

Huang, H.-C., Chen, L.-C., Lin, S.-B., & Chen, H.-H. (2011). Nano-biomaterials application: In situ modification of bacterial cellulose structure by adding HPMC during fermentation. *Carbohydrate Polymers*, *83*(2), 979–987.

Huang, Y., Wang, T., Ji, M., Yang, J., Zhu, C., & Sun, D. (2014). Simple preparation of carbonized bacterial cellulose-Pt composite as a high performance electrocatalyst for direct methanol fuel cells (DMFC). *Materials Letters*, *128*, 93–96.

Huang, Y., Lin, Z., Zheng, M., Wang, T., Yang, J., Yuan, F., et al. (2016). Amorphous Fe2O3 nanoshells coated on carbonized bacterial cellulose nanofibers as a flexible anode for high-performance lithium ion batteries. *Journal of Power Sources*, *307*, 649–656.

Huang, C., Yang, X. Y., Xiong, L., Guo, H. J., Luo, J., Wang, B., et al. (2015). Evaluating the possibility of using acetone-butanol-ethanol (ABE) fermentation wastewater for bacterial cellulose production by Gluconacetobacter xylinus. *Letters in Applied Microbiology*, *60*(5), 491–496.

Huang, Y., Zheng, M., Lin, Z., Zhao, B., Zhang, S., Yang, J., et al. (2015). Flexible cathodes and multifunctional interlayers based on carbonized bacterial cellulose for high-performance lithium-sulfur batteries. *Journal of Materials Chemistry A*, *3*(20), 10910–10918.

Hussein, M., Yahaya, A., Ling, P., & Long, C. (2005). Acetobacter xylenium as a shape-directing agent for the formation of nano-, micro-sized zinc oxide. *Journal of Materials Science*, *40*(23), 6325–6328.

Hyun, J. Y., Mahanty, B., & Kim, C. G. (2014). Utilization of makgeolli sludge filtrate (MSF) as low-cost substrate for bacterial cellulose production by gluconacetobacter xylinus. *Applied Biochemistry and Biotechnology*, *172*(8), 3748–3760.

Ifuku, S., Nogi, M., Abe, K., Handa, K., Nakatsubo, F., & Yano, H. (2007). Surface modification of bacterial cellulose nanofibers for property enhancement of optically transparent composites: Dependence on acetyl-group DS. *Biomacromolecules*, *8*(6), 1973–1978.

Ishikawa, A., Okano, T., & Sugiyama, J. (1997). Fine structure and tensile properties of ramie fibres in the crystalline form of cellulose I, II, IIII and IVI. *Polymer*, *38*(2), 463–468.

Isogai, A., & Kato, Y. (1998). Preparation of polyuronic acid from cellulose by TEMPO-mediated oxidation. *Cellulose*, *5*(3), 153–164.

Isogai, A., Saito, T., & Fukuzumi, H. (2011). TEMPO-oxidized cellulose nanofibers. *Nanoscale*, *3*(1), 71–85.

Jahn, C. E., Selimi, D. A., Barak, J. D., & Charkowski, A. O. (2011). The Dickeya dadantii biofilm matrix consists of cellulose nanofibres, and is an emergent property dependent upon the type III secretion system and the cellulose synthesis operon. *Microbiology*, *157*(10), 2733–2744.

Janpetch, N., Saito, N., & Rujiravanit, R. (2016). Fabrication of bacterial cellulose-ZnO composite via solution plasma process for antibacterial applications. *Carbohydrate Polymers*, *148*, 335–344.

Jiang, G., Qiao, J., & Hong, F. (2012). Application of phosphoric acid and phytic acid-doped bacterial cellulose as novel proton-conducting membranes to PEMFC. *International Journal of Hydrogen Energy*, *37*(11), 9182–9192.

Jiang, F., Yin, L., Yu, Q., Zhong, C., & Zhang, J. (2015). Bacterial cellulose nanofibrous membrane as thermal stable separator for lithium-ion batteries. *Journal of Power Sources*, *279*, 21–27.

Jiang, F., Nie, Y., Yin, L., Feng, Y., Yu, Q., & Zhong, C. (2016). Core-shell-structured nanofibrous membrane as advanced separator for lithium-ion batteries. *Journal of Membrane Science*, *510*, 1–9.

Jinmin, Q., Zhiyu, Q., Xueqiong, Y., Qinhuan, Z., & Li, Z. (2015). Synthesis and characterization of alkylated bacterial cellulose in an ionic liquid. *Bioresources*, *10*(2), 2185–2194.

Johnson, L., Thielemans, W., & Walsh, D. A. (2011). Synthesis of carbon-supported Pt nanoparticle electrocatalysts using nanocrystalline cellulose as reducing agent. *Green Chemistry*, *13*(7), 1686–1693.

Kang, Y. J., Chun, S.-J., Lee, S.-S., Kim, B.-Y., Kim, J. H., Chung, H., et al. (2012). All-solid-state flexible supercapacitors fabricated with bacterial nanocellulose papers, carbon nanotubes, and triblock-copolymer ion gels. *ACS Nano*, *6*(7), 6400–6406.

Khandelwal, M., & Windle, A. H. (2014). Small angle X-ray study of cellulose macromolecules produced by tunicates and bacteria. *International Journal of Biological Macromolecules*, *68*, 215–217.

Kim, D.-Y., Nishiyama, Y., & Kuga, S. (2002). Surface acetylation of bacterial cellulose. *Cellulose*, *9*(3), 361–367.

Kim, S.-S., Jeon, J.-H., Kim, H.-I., Kee, C. D., & Oh, I.-K. (2015). High-fidelity bioelectronic muscular actuator based on graphene-Mediated and TEMPO-oxidized bacterial cellulose. *Advanced Functional Materials*, *25*(23), 3560–3570.

Klemm, D., Kramer, F., Moritz, S., Lindström, T., Ankerfors, M., Gray, D., et al. (2011). Nanocelluloses: A new family of nature-based materials. *Angewandte Chemie International Edition*, *50*(24), 5438–5466.

Kuga, S., Kim, D.-Y., Nishiyama, Y., & Brown, R. M. (2002). Nanofibrillar carbon from native cellulose. *Molecular Crystals and Liquid Crystals*, *387*(1), 13–19.

Łaskiewicz, B. (1998). Solubility of bacterial cellulose and its structural properties. *Journal of Applied Polymer Science*, *67*(11), 1871–1876.

Lai, C., Zhang, S. J., Wang, L. Q., Sheng, L. Y., Zhou, Q. Z., & Xi, T. F. (2015). The relationship between microstructure and in vivo degradation of modified bacterial cellulose sponges. *Journal of Materials Chemistry B*, *3*(46), 9001–9010.

Lai, C., Sheng, L., Liao, S., Xi, T., & Zhang, Z. (2013). Surface characterization of TEMPO-oxidized bacterial cellulose. *Surface and Interface Analysis*, *45*(11–12), 1673–1679.

Lai, F., Miao, Y.-E., Huang, Y., Zhang, Y., & Liu, T. (2016). Nitrogen-doped carbon nanofiber/molybdenum disulfide nanocomposites derived from bacterial cellulose for high-Efficiency electrocatalytic hydrogen evolution reaction. *ACS Applied Materials & Interfaces*.

Lai, C., Zhang, S., Sheng, L., Liao, S., Xi, T., & Zhang, Z. (2013). TEMPO-mediated oxidation of bacterial cellulose in a bromide-free system. *Colloid and Polymer Science*, *291*(12), 2985–2992.

Lee, K.-Y., Quero, F., Blaker, J., Hill, C. S., Eichhorn, S., & Bismarck, A. (2011). Surface only modification of bacterial cellulose nanofibres with organic acids. *Cellulose*, *18*(3), 595–605.

Lei, W., Han, L., Xuan, C., Lin, R., Liu, H., Xin, H. L., et al. (2016). Nitrogen-doped carbon nanofibers derived from polypyrrole coated bacterial cellulose as high-performance electrode materials for supercapacitors and Li-ion batteries. *Electrochimica Acta*, *210*, 130–137.

Li, Z., Friedrich, A., & Taubert, A. (2008). Gold microcrystal synthesis via reduction of HAuCl4 by cellulose in the ionic liquid 1-butyl-3-methyl imidazolium chloride. *Journal of Materials Chemistry*, *18*(9), 1008–1014.

Li, Z., Ottmann, A., Thauer, E., Neef, C., Sai, H., Sun, Q., et al. (2016). A facile synthesis method and electrochemical studies of a hierarchical structured MoS2/C-nanocomposite. *RSC Advances*, *6*(79), 76084–76092.

Li, J., Wan, Y., Li, L., Liang, H., & Wang, J. (2009). Preparation and characterization of 2,3-dialdehyde bacterial cellulose for potential biodegradable tissue engineering scaffolds. *Materials Science and Engineering: C*, *29*(5), 1635–1642.

Li, X., Chen, S., Hu, W., Shi, S., Shen, W., Zhang, X., et al. (2009). In situ synthesis of CdS nanoparticles on bacterial cellulose nanofibers. *Carbohydrate Polymers*, *76*(4), 509–512.

Liang, H.-W., Wu, Z.-Y., Chen, L.-F., Li, C., & Yu, S.-H. (2015). Bacterial cellulose derived nitrogen-doped carbon nanofiber aerogel: An efficient metal-free oxygen reduction electrocatalyst for zinc-air battery. *Nano Energy*, *11*, 366–376.

Liebner, F., Haimer, E., Wendland, M., Neouze, M.-A., Schlufter, K., Miethe, P., et al. (2010). Aerogels from unaltered bacterial cellulose: Application of scCO2 drying for the preparation of shaped, ultra-lightweight cellulosic aerogels. *Macromolecular Bioscience*, *10*(4), 349–352.

Lin, N., & Dufresne, A. (2014). Nanocellulose in biomedicine: Current status and future prospect. *European Polymer Journal*, *59*, 302–325.

Liu, S., Yan, W., Cao, X., Zhou, Z., & Yang, R. (2016). Bacterial-cellulose-derived carbon nanofiber-supported CoFe2O4 as efficient electrocatalyst for oxygen reduction and evolution reactions. *International Journal of Hydrogen Energy*, *41*(11), 5351–5360.

Liu, X., Jiang, H., Ge, W., Wu, C., Chen, D., Li, Q., et al. (2015). Green and facile synthesis of highly biocompatible carbon nanospheres and their pH-responsive delivery of doxorubicin to cancer cells. *RSC Advances*, *5*(23), 17532–17540.

Liu, Y., Zhou, J., Zhu, E., Tang, J., Liu, X., & Tang, W. (2015). Facile synthesis of bacterial cellulose fibres covalently intercalated with graphene oxide by one-step cross-linking for robust supercapacitors. *Journal of Materials Chemistry C*, *3*(5), 1011–1017.

Lu, X., & Shen, X. (2011). Solubility of bacteria cellulose in zinc chloride aqueous solutions. *Carbohydrate Polymers*, *86*(1), 239–244.

Luo, H., Xiong, G., Hu, D., Ren, K., Yao, F., Zhu, Y., et al. (2013). Characterization of TEMPO-oxidized bacterial cellulose scaffolds for tissue engineering applications. *Materials Chemistry and Physics*, *143*(1), 373–379.

Luo, H., Ji, D., Li, W., Xiao, J., Li, C., Xiong, G., et al. (2016). Constructing a highly bioactive 3D nanofibrous bioglass scaffold via bacterial cellulose-templated sol-gel approach. *Materials Chemistry and Physics*, *176*, 1–5.

Lv, P., Wei, A., Wang, Y., Li, D., Zhang, J., Lucia, L. A., et al. (2016). Copper nanoparticles-sputtered bacterial cellulose nanocomposites displaying enhanced electromagnetic shielding, thermal, conduction, and mechanical properties. *Cellulose*, 1–11.

Mühlethaler, K. (1949). The structure of bacterial cellulose. *Biochimica Et Biophysica Acta*, *3*, 527–535.

Müller, D., Rambo, C. R., Recouvreux, D. O. S., Porto, L. M., & Barra, G. M. O. (2011). Chemical in situ polymerization of polypyrrole on bacterial cellulose nanofibers. *Synthetic Metals*, *161*(1–2), 106–111.

Ma, B., Huang, Y., Zhu, C., Chen, C., Fan, M., & Sun, D. (2016). A facile method to synthesize carbon coated Fe, Co and Ni and an examination of their magnetic properties. *Journal of Alloys and Compounds*, *687*, 741–745.

Maeda, H., Nakajima, M., Hagiwara, T., Sawaguchi, T., & Yano, S. (2006). Bacterial cellulose/silica hybrid fabricated by mimicking biocomposites. *Journal of Materials Science*, *41*(17), 5646–5656.

Martinez-Sanz, M., Lopez-Rubio, A., & Lagaron, J. M. (2011). Optimization of the nanofabrication by acid hydrolysis of bacterial cellulose nanowhiskers. *Carbohydrate Polymers*, *85*(1), 228–236.

Menchaca-Nal, S., Londono-Calderon, C. L., Cerrutti, P., Foresti, M. L., Pampillo, L., Bilovol, V., et al. (2016). Facile synthesis of cobalt ferrite nanotubes using bacterial nanocellulose as template. *Carbohydrate Polymers*, *137*, 726–731.

Mi, Y., Wen, L., Wang, Z., Cao, D., Zhao, H., Zhou, Y., et al. (2016). Ultra-low mass loading of platinum nanoparticles on bacterial cellulose derived carbon nanofibers for efficient hydrogen evolution. *Catalysis Today*, *262*, 141–145.

Mochochoko, T., Oluwafemi, O. S., Jumbam, D. N., & Songca, S. P. (2013). Green synthesis of silver nanoparticles using cellulose extracted from an aquatic weed; water hyacinth. *Carbohydrate Polymers*, *98*(1), 290–294.

Mohammadkazemi, F., Faria, M., & Cordeiro, N. (2013). In situ biosynthesis of bacterial nanocellulose-CaCO3 hybrid bionanocomposite: One-step process. *Materials Science and Engineering: C*, *65*, 393–399.

Molina de Olyveira, G., Maria Manzine Costa, L., & Basmaji, P. (2013). Physically modified bacterial cellulose as alternative routes for transdermal drug delivery. *Journal of Biomaterials and Tissue Engineering*, *3*(2), 227–232.

Moon, S.-H., Park, J.-M., Chun, H.-Y., & Kim, S.-J. (2006). Comparisons of physical properties of bacterial celluloses produced in different culture conditions using saccharified food wastes. *Biotechnology and Bioprocess Engineering*, *11*(1), 26–31.

Moon, R. J., Martini, A., Nairn, J., Simonsen, J., & Youngblood, J. (2011). Cellulose nanomaterials review: Structure, properties and nanocomposites. *Chemical Society Reviews*, *40*(7), 3941–3994.

Morales-Narvez, E., Golmohammadi, H., Naghdi, T., Yousefi, H., Kostiv, U., Horak, D., et al. (2015). Nanopaper as an optical sensing platform. *ACS Nano*, *9*(7), 7296–7305.

Nata, I. F., & Lee, C. K. (2010). Novel carbonaceous nanocomposite pellicle based on bacterial cellulose. *Green Chemistry*, *12*(8), 1454–1459.

Nata, I. F., Sureshkumar, M., & Lee, C.-K. (2011). One-pot preparation of amine-rich magnetite/bacterial cellulose nanocomposite and its application for arsenate removal. *RSC Advances*, *1*(4), 625–631.

Nge, T. T., & Sugiyama, J. (2007). Surface functional group dependent apatite formation on bacterial cellulose microfibrils network in a simulated body fluid. *Journal of Biomedical Materials Research Part A*, *81A*(1), 124–134.

Okushita, K., Chikayama, E., & Kikuchi, J. (2012). Solubilization mechanism and characterization of the structural change of bacterial cellulose in regenerated states through ionic liquid treatment. *Biomacromolecules*, *13*(5), 1323–1330.

Oliveira, R., Silva Barud, H., Assunçao, R., Silva Meireles, C., Carvalho, G., Filho, G., et al. (2011). Synthesis and characterization of microcrystalline cellulose produced from bacterial cellulose. *Journal of Thermal Analysis & Calorimetry*, *106*(3), 703–709.

Oshima, T., Kondo, K., Ohto, K., Inoue, K., & Baba, Y. (2008). Preparation of phosphorylated bacterial cellulose as an adsorbent for metal ions. *Reactive and Functional Polymers*, *68*(1), 376–383.

Osorio M., Restrepo D., Castro C., Montoya U., Zuluaga R., Ganan P. (2013). In Laudon Matthew, Romanowicz Bart (eds.) From Nanotech Conference & Expo 2013: *An Interdisciplinary Integrative Forum on Nanotechnology, Microtechnology, Biotechnology and Cleantechnology*, Washington, DC, United States, May 12-16, 2013, 1, (pp.774-776).

Park, M., Lee, D., & Hyun, J. (2015). Nanocellulose-alginate hydrogel for cell encapsulation. *Carbohydrate Polymers*, *116*, 223–228.

Park, M., Lee, D., Shin, S., & Hyun, J. (2015). Effect of negatively charged cellulose nanofibers on the dispersion of hydroxyapatite nanoparticles for scaffolds in bone tissue engineering. *Colloids and Surfaces B: Biointerfaces*, *130*, 222–228.

Paximada, P., Dimitrakopoulou, E. A., Tsouko, E., Koutinas, A. A., Fasseas, C., & Mandala, I. G. (2016). Structural modification of bacterial cellulose fibrils under ultrasonic irradiation. *Carbohydrate Polymers*, *150*, 5–12.

Pekala, R. W., Alviso, C. T., & LeMay, J. D. (1990). Organic aerogels: Microstructural dependence of mechanical properties in compression. *Journal of Non-Crystalline Solids*, *125*(1), 67–75.

Peng, S., Zheng, Y., Wu, J., Wu, Y., Ma, Y., Song, W., et al. (2011). Preparation and characterization of degradable oxidized bacterial cellulose reacted with nitrogen dioxide. *Polymer Bulletin*, *68*(2), 415–423.

Peng, Y., Gardner, D., Han, Y., Kiziltas, A., Cai, Z., & Tshabalala, M. (2013). Influence of drying method on the material properties of nanocellulose I: Thermostability and crystallinity. *Cellulose*, *20*(5), 2379–2392.

Phisalaphong, M., Suwanmajo, T., & Sangtherapitikul, P. (2008). Novel nanoporous membranes from regenerated bacterial cellulose. *Journal of Applied Polymer Science*, *107*(1), 292–299.

Pinto, R. J. B., Neves, M. C., Neto, C. P., & Trindade, T. (2012). Growth and chemical stability of copper nanostructures on cellulosic fibers. *European Journal of Inorganic Chemistry*, *2012*(31), 5043–5049.

Pourreza, N., Golmohammadi, H., Naghdi, T., & Yousefi, H. (2015). Green in-situ synthesized silver nanoparticles embedded in bacterial cellulose nanopaper as a bionanocomposite plasmonic sensor. *Biosensors and Bioelectronics*, *74*, 353–359.

Qin, Z., Ji, L., Yin, X., Zhu, L., Lin, Q., & Qin, J. (2014). Synthesis and characterization of bacterial cellulose sulfates using a SO3/pyridine complex in DMAc/LiCl. *Carbohydrate Polymers*, *101*, 947–953.

Römling, U., & Galperin, M. Y. (2015). Bacterial cellulose biosynthesis: Diversity of operons, subunits, products, and functions. *Trends in Microbiology*, *23*(9), 545–557.

Rani, M. U., Rastogi, N. K., & Appaiah, K. A. A. (2011). Statistical optimization of medium composition for bacterial cellulose production by gluconacetobacter hansenii UAC09 using coffee cherry husk extract – an agro-Industry waste. *Journal of Microbiology and Biotechnology*, *21*(7), 739–745.

Rani, M. U., Udayasankar, K., & Appaiah, K. A. A. (2011). Properties of bacterial cellulose produced in grape medium by native isolate Gluconacetobacter sp. *Journal of Applied Polymer Science*, *120*(5), 2835–2841.

Rieger, K. A., Cho, H. J., Yeung, H. F., Fan, W., & Schiffman, J. D. (2016). Antimicrobial activity of silver ions released from zeolites immobilized on cellulose nanofiber mats. *ACS Applied Materials & Interfaces*, *8*(5), 3032–3040.

Roman, M., & Winter, W. T. (2004). Effect of sulfate groups from sulfuric acid hydrolysis on the thermal degradation behavior of bacterial cellulose. *Biomacromolecules*, *5*(5), 1671–1677.

Ruka, D. R., Simon, G. P., & Dean, K. M. (2012). Altering the growth conditions of Gluconacetobacter xylinus to maximize the yield of bacterial cellulose. *Carbohydrate Polymers*, *89*(2), 613–622.

Ruka, D. R., Simon, G. P., & Dean, K. M. (2013). In situ modifications to bacterial cellulose with the water insoluble polymer poly-3-hydroxybutyrate. *Carbohydrate Polymers*, *92*(2), 1717–1723.

Russler, A., Wieland, M., Bacher, M., Henniges, U., Miethe, P., Liebner, F., et al. (2012). AKD-modification of bacterial cellulose aerogels in supercritical CO2. *Cellulose*, *19*(4), 1337–1349.

Sai, H., Fu, R., Xing, L., Xiang, J., Li, Z., Li, F., et al. (2015). Surface modification of bacterial cellulose aerogels: Web-like skeleton for oil/water separation. *ACS Applied Materials & Interfaces*, *7*(13), 7373–7381.

Sai, H., Xing, L., Xiang, J., Cui, L., Jiao, J., Zhao, C., et al. (2015). Flexible aerogels based on an interpenetrating network of bacterial cellulose and silica by a non-supercritical drying process. *Journal of Materials Chemistry A*, *1*(27), 7963–7970.

Saito, T., Nishiyama, Y., Putaux, J.-L., Vignon, M., & Isogai, A. (2006). Homogeneous suspensions of individualized microfibrils from TEMPO-catalyzed oxidation of native cellulose. *Biomacromolecules*, *7*(6), 1687–1691.

Salon, M.-C. B., Gerbaud, G., Abdelmouleh, M., Bruzzese, C., Boufi, S., & Belgacem, M. N. (2007). Studies of interactions between silane coupling agents and cellulose fibers with liquid and solid-state NMR. *Magnetic Resonance in Chemistry*, *45*(6), 473–483.

Schlufter, K., Schmauder, H.-P., Dorn, S., & Heinze, T. (2006). Efficient homogeneous chemical modification of bacterial cellulose in the ionic liquid 1-*N*-Butyl-3-methylimidazolium chloride. *Macromolecular Rapid Communications*, *27*(19), 1670–1676.

Sehaqui, H., Zhou, Q., Ikkala, O., & Berglund, L. A. (2011). Strong and tough cellulose nanopaper with high specific surface area and porosity. *Biomacromolecules*, *12*(10), 3638–3644.

Shah, J., & Brown, R. M., Jr. (2005). Towards electronic paper displays made from microbial cellulose. *Applied Microbiology & Biotechnology*, *66*(4), 352–355.

Shah, N., Ul-Islam, M., Khattak, W. A., & Park, J. K. (2013). Overview of bacterial cellulose composites: A multipurpose advanced material. *Carbohydrate Polymers*, *98*(2), 1585–1598.

Shahmohammadi Jebel, F., & Almasi, H. (2016). Morphological, physical, antimicrobial and release properties of ZnO nanoparticles-loaded bacterial cellulose films. *Carbohydrate Polymers*, *149*, 8–19.

Shan, D., Yang, J., Liu, W., Yan, J., & Fan, Z. (2016). Biomass-derived three-dimensional honeycomb-like hierarchical structured carbon for ultrahigh energy density asymmetric supercapacitors. *Journal of Materials Chemistry A*.

Shao, W., Wang, S., Wu, J., Huang, M., Liu, H., & Min, H. (2016). Synthesis and antimicrobial activity of copper nanoparticle loaded regenerated bacterial cellulose membranes. *RSC Advances*, *6*(70), 65879–65884.

Shen, X., Ji, Y., Wang, D., & Yang, Q. (2010). Solubility of a high molecular-weight bacterial cellulose in lithium chloride/*N*,*N*-dimethylacetamide solution. *Journal of Macromolecular Science Part B*, *49*(5), 1012–1018.

Shi, Q. S., Feng, J., Li, W. R., Zhou, G., Chen, A. M., Ouyang, Y. S., et al. (2013). Effect of different conditions on the average degree of polymerization of bacterial cellulose produced by Gluconacetobacter intermedius BC-41. *Cellulose Chemistry and Technology*, *47*, 503–508.

Shi, X., Cui, Q., Zheng, Y., Peng, S., Wang, G., & Xie, Y. (2014). Effect of selective oxidation of bacterial cellulose on degradability in phosphate buffer solution and their affinity for epidermal cell attachment. *RSC Advances*, *4*(105), 60749–60756.

Shibazaki, H., Kuga, S., & Okano, T. (1997). Mercerization and acid hydrolysis of bacterial cellulose. *Cellulose*, *4*(2), 75–87.

Shibazaki, H., Saito, M., Kuga, S., & Okano, T. (1998). Native cellulose II production by acetobacter xylinum under physical constraints. *Cellulose*, *5*(3), 165–173.

Shimizu, K., Imai, H., Hirashima, H., & Tsukuma, K. (1999). Low-temperature synthesis of anatase thin films on glass and organic substrates by direct deposition from aqueous solutions. *Thin Solid Films*, *351*(1–2), 220–224.

Stoica-Guzun, A., Stroescu, M., Jinga, S. I., Mihalache, N., Botez, A., Matei, C., et al. (2016). Box-Behnken experimental design for chromium(VI) ions removal by bacterial cellulose-magnetite composites. *International Journal of Biological Macromolecules*, *91*, 1062–1072.

Su, Y., Burger, C., Ma, H., Chu, B., & Hsiao, B. S. (2015). Morphological and property investigations of carboxylated cellulose nanofibers extracted from different biological species. *Cellulose*, *22*(5), 3127–3135.

Sulaeva, I., Henniges, U., Rosenau, T., & Potthast, A. (2015). Bacterial cellulose as a material for wound treatment: Properties and modifications. A review. *Biotechnology Advances*, *33*(8), 1547–1571.

Sun, D., Yang, J., Li, J., Yu, J., Xu, X., & Yang, X. (2010). Novel Pd-Cu/bacterial cellulose nanofibers: Preparation and excellent performance in catalytic denitrification. *Applied Surface Science*, *256*(7), 2241–2244.

Sun, Y., Wang, X., Ding, C., Cheng, W., Chen, C., Hayat, T., et al. (2016). Direct synthesis of bacteria-derived carbonaceous nanofibers as a highly efficient material for radionuclides elimination. *ACS Sustainable Chemistry & Engineering*.

Sun, D., Yang, J., & Wang, X. (2010). Bacterial cellulose/TiO2 hybrid nanofibers prepared by the surface hydrolysis method with molecular precision. *Nanoscale*, *2*(2), 287–292.

Suwanposri, A., Yukphan, P., Yamada, Y., & Ochaikul, D. (2014). Statistical optimisation of culture conditions for biocellulose production by Komagataeibacter sp. PAP1 using soya bean whey. *Maejo International Journal of Science and Technology*, *8*(1), 1–14.

Tang, K., Fu, L., White, R. J., Yu, L., Titirici, M.-M., Antonietti, M., et al. (2012). Hollow carbon nanospheres with superior rate capability for sodium-based batteries. *Advanced Energy Materials*, *2*(7), 873–877.

Tercjak, A., Gutierrez, J., Barud, H. S., Domeneguetti, R. R., & Ribeiro, S. J. L. (2015). Nano- and macroscale structural and mechanical properties of in situ synthesized bacterial cellulose/PEO-b-PPO-b-PEO biocomposites. *ACS Applied Materials & Interfaces*, *7*(7), 4142–4150.

Tischer, P. C. S. F., Sierakowski, M. R., Westfahl, H., & Tischer, C. A. (2010). Nanostructural reorganization of bacterial cellulose by ultrasonic treatment. *Biomacromolecules*, *11*(5), 1217–1224.

Tobjörk, D., & Österbacka, R. (2011). Paper electronics. *Advanced Materials*, *23*(17), 1935–1961.

Tokoh, C., Takabe, K., Fujita, M., & Saiki, H. (1998). Cellulose synthesized by acetobacter xylinum in the presence of acetyl glucomannan. *Cellulose*, *5*(4), 249–261.

Tomé, L. C., Freire, M. G., Rebelo, L. P. N., Silvestre, A. J. D., Neto, C. P., Marrucho, I. M., et al. (2011). Surface hydrophobization of bacterial and vegetable cellulose fibers using ionic liquids as solvent media and catalysts. *Green Chemistry*, *13*(9), 2464–2470.

Tong, S., Zheng, M., Lu, Y., Lin, Z., Zhang, X., He, P., et al. (2015). Binder-free carbonized bacterial cellulose-supported ruthenium nanoparticles for Li-O2 batteries. *Chemical Communications*, *51*(34), 7302–7304.

Tsouko, E., Kourmentza, C., Ladakis, D., Kopsahelis, N., Mandala, I., Papanikolaou, S., et al. (2015). Bacterial cellulose production from industrial waste and by-product streams. *International Journal of Molecular Sciences*, *16*(7), 14832.

Uhlin, K. I., Atalla, R. H., & Thompson, N. S. (1995). Influence of hemicelluloses on the aggregation patterns of bacterial cellulose. *Cellulose*, *2*(2), 129–144.

Ul-Islam, M., Khan, S., Ullah, M. W., & Park, J. K. (2015). Bacterial cellulose composites: Synthetic strategies and multiple applications in bio-medical and electro-conductive fields. *Biotechnology Journal*, *10*(12), 1847–1861.

Vazquez, A., Foresti, M. L., Cerrutti, P., & Galvagno, M. (2013). Bacterial cellulose from simple and low cost production media by gluconacetobacter xylinus. *Journal of Polymers and the Environment*, *21*(2), 545–554.

Wan, Y., Zuo, G., Yu, F., Huang, Y., Ren, K., & Luo, H. (2011). Preparation and mineralization of three-dimensional carbon nanofibers from bacterial cellulose as potential scaffolds for bone tissue engineering. *Surface and Coatings Technology*, *205*(8–9), 2938–2946.

Wan, Y., Yang, Z., Xiong, G., Guo, R., Liu, Z., & Luo, H. (2015). Anchoring Fe3O4 nanoparticles on three-dimensional carbon nanofibers toward flexible high-performance anodes for lithium-ion batteries. *Journal of Power Sources*, *294*, 414–419.

Wan, Y., Yang, Z., Xiong, G., & Luo, H. (2015). A general strategy of decorating 3D carbon nanofiber aerogels derived from bacterial cellulose with nano-Fe3O4 for high-performance flexible and binder-free lithium-ion battery anodes. *Journal of Materials Chemistry A*, *3*(30), 15386–15393.

Wang, P., Geng, Z., Gao, J., Xuan, R., Liu, P., Wang, Y., et al. (2015). ZnxCd1-xS/bacterial cellulose bionanocomposite foams with hierarchical architecture and enhanced visible-light photocatalytic hydrogen production activity. *Journal of Materials Chemistry A*, *3*(4), 1709–1716.

Wang, Y.-Y., Hou, B.-H., Lu, H.-Y., Wan, F., Wang, J., & Wu, X.-L. (2015). Porous N-doped carbon material derived from prolific chitosan biomass as a high-performance electrode for energy storage. *RSC Advances*, *5*(118), 97427–97434.

Wang, X., Kong, D., Zhang, Y., Wang, B., Li, X., Qiu, T., et al. (2016). All-biomaterial supercapacitor derived from bacterial cellulose. *Nanoscale*, *8*(17), 9146–9150.

Wang, W., Li, H.-Y., Zhang, D.-W., Jiang, J., Cui, Y.-R., Qiu, S., et al. (2010). Fabrication of bienzymatic glucose biosensor based on novel gold nanoparticles-bacteria cellulose nanofibers nanocomposite. *Electroanalysis*, *22*(21), 2543–2550.

Wang, B., Li, X., Luo, B., Yang, J., Wang, X., Song, Q., et al. (2013). Pyrolyzed bacterial cellulose: A versatile support for lithium ion battery anode materials. *Small*, *9*(14), 2399–2404.

Wang, L., Schutz, C., Salazar-Alvarez, G., & Titirici, M.-M. (2014). Carbon aerogels from bacterial nanocellulose as anodes for lithium ion batteries. *RSC Advances*, *4*(34), 17549–17554.

Wang, W., Sun, Y., Liu, B., Wang, S., & Cao, M. (2015). Porous carbon nanofiber webs derived from bacterial cellulose as an anode for high performance lithium ion batteries. *Carbon*, *91*, 56–65.

Wang, H., Yu, J., Zhao, Y., & Guo, Q. (2013). A facile route for PbO@C nanocomposites: An electrode candidate for lead-acid batteries with enhanced capacitance. *Journal of Power Sources*, *224*, 125–131.

Wang, P., Zhao, J., Xuan, R., Wang, Y., Zou, C., Zhang, Z., et al. (2014). Flexible and monolithic zinc oxide bionanocomposite foams by a bacterial cellulose mediated approach for antibacterial applications. *Dalton Transactions*, *43*(18), 6762–6768.

Watanabe, K., Tabuchi, M., Morinaga, Y., & Yoshinaga, F. (1998). Structural features and properties of bacterial cellulose produced in agitated culture. *Cellulose*, *5*(3), 187–200.

Wesarg, F., Schlott, F., Grabow, J., Heinz-Dieter, K., Heßler, N., Kralisch, D., et al. (2012). In situ synthesis of photocatalytically active hybrids consisting of bacterial nanocellulose and anatase nanoparticles. *Langmuir*, *28*(37), 13518–13525.

Wilamowska, M., Graczyk-Zajac, M., & Riedel, R. (2013). Composite materials based on polymer-derived SiCN ceramic and disordered hard carbons as anodes for lithium-ion batteries. *Journal of Power Sources*, *244*, 80–86.

Witter, R., Sternberg, U., Hesse, S., Kondo, T., Koch, F.-T., & Ulrich, A. S. (2006). 13C chemical shift constrained crystal structure refinement of cellulose Iβ and its verification by NMR anisotropy experiments. *Macromolecules*, *39*(18), 6125–6132.

Wong, S.-S., Kasapis, S., & Tan, Y. M. (2009). Bacterial and plant cellulose modification using ultrasound irradiation. *Carbohydrate Polymers*, *77*(2), 280–287.

Wu, J., Zheng, Y., Yang, Z., Cui, Q., Wang, Q., Gao, S., et al. (2012). Chemical modifications and characteristic changes in bacterial cellulose treated with different media. *Journal of Polymer Research*, *19*(9), 1–8.

Wu, T. X., Wang, G. Z., Zhang, X., Chen, C., Zhang, Y. X., & Zhao, H. J. (2015). Transforming chitosan into N-doped graphitic carbon electrocatalysts. *Chemical Communications*, *51*(7), 1334–1337.

Wu, Z.-Y., Li, C., Liang, H.-W., Chen, J.-F., & Yu, S.-H. (2013). Ultralight, flexible, and fire-Resistant carbon nanofiber aerogels from bacterial cellulose. *Angewandte Chemie International Edition*, *52*(10), 2925–2929.

Wu, Z.-Y., Liang, H.-W., Chen, L.-F., Hu, B.-C., & Yu, S.-H. (2016). Bacterial cellulose: A robust platform for design of three dimensional carbon-Based functional nanomaterials. *Accounts of Chemical Research*, *49*(1), 96–105.

Yang, J., Sun, D., Li, J., Yang, X., Yu, J., Hao, Q., et al. (2009). In situ deposition of platinum nanoparticles on bacterial cellulose membranes and evaluation of PEM fuel cell performance. *Electrochimica Acta*, *54*(26), 6300–6305.
Yang, J., Yu, J., Fan, J., Sun, D., Tang, W., & Yang, X. (2011). Biotemplated preparation of CdS nanoparticles/bacterial cellulose hybrid nanofibers for photocatalysis application. *Journal of Hazardous Materials*, *189*(1–2), 377–383.
Yang, Z., Chen, S., Hu, W., Yin, N., Zhang, W., Xiang, C., et al. (2012). Flexible luminescent CdSe/bacterial cellulose nanocomoposite membranes. *Carbohydrate Polymers*, *88*(1), 173–178.
Yang, X. Y., Huang, C., Guo, H. J., Xiong, L., Li, Y. Y., Zhang, H. R., et al. (2013). Bioconversion of elephant grass (Pennisetum purpureum) acid hydrolysate to bacterial cellulose by Gluconacetobacter xylinus. *Journal of Applied Microbiology*, *115*(4), 995–1002.
Ye, T.-N., Lv, L.-B., Li, X.-H., Xu, M., & Chen, J.-S. (2014). Strongly veined carbon nanoleaves as a highly efficient metal-Free electrocatalyst. *Angewandte Chemie International Edition*, *53*(27), 6905–6909.
Yin, J., Gao, F., Wu, Y., Wang, J., & Lu, Q. (2010). Synthesis of Mn3O4 octahedrons and other manganese-based nanostructures through a simple and green route. *CrystEngComm*, *12*(11), 3401–3403.
Yoshida, Y., Heux, L., & Isogai, A. (2012). Heterogeneous reaction between cellulose and alkyl ketene dimer under solvent-free conditions. *Cellulose*, *19*(5), 1667–1676.
Yu, X., & Atalla, R. H. (1996). Production of cellulose II by Acetobacter xylinum in the presence of 2,6-dichlorobenzonitrile. *International Journal of Biological Macromolecules*, *19*(2), 145–146.
Zeng, M., Laromaine, A., Feng, W., Levkin, P. A., & Roig, A. (2014). Origami magnetic cellulose: Controlled magnetic fraction and patterning of flexible bacterial cellulose. *Journal of Materials Chemistry C*, *2*(31), 6312–6318.
Zeng, M., Laromaine, A., & Roig, A. (2014). Bacterial cellulose films: Influence of bacterial strain and drying route on film properties. *Cellulose*, *21*(6), 4455–4469.
Zhang, D., & Qi, L. (2005). Synthesis of mesoporous titania networks consisting of anatase nanowires by templating of bacterial cellulose membranes. *Chemical Communications (Cambridge, United Kingdom)*, *21*, 2735–2737.
Zhang, T., Wang, W., Zhang, D., Zhang, X., Ma, Y., Zhou, Y., et al. (2010). Biotemplated synthesis of gold nanoparticle–bacteria cellulose nanofiber nanocomposites and their application in biosensing. *Advanced Functional Materials*, *20*(7), 1152–1160.
Zhang, G., Liao, Q., Zhang, Z., Liang, Q., Zhao, Y., Zheng, X., et al. (2016). Novel piezoelectric paper-based flexible nanogenerators composed of BaTiO3 nanoparticles and bacterial cellulose. *Advanced Science*, *3*(2), n/a–n/a.
Zhang, Z., Zhang, J., Zhao, X., & Yang, F. (2015). Core-sheath structured porous carbon nanofiber composite anode material derived from bacterial cellulose/polypyrrole as an anode for sodium-ion batteries. *Carbon*, *95*, 552–559.
Zhang, T., Zheng, Y., Liu, S., Yue, L., Gao, Y., & Yao, Y. (2015). Bacterial cellulose membrane supported three-dimensionally dispersed silver nanoparticles used as membrane electrode for oxygen reduction reaction in phosphate buffered saline. *Journal of Electroanalytical Chemistry*, *750*, 43–48.
Zheng, W., Chen, S., Zhao, S., Zheng, Y., & Wang, H. (2014). Zinc sulfide nanoparticles template by bacterial cellulose and their optical properties. *Journal of Applied Polymer Science*, *131*(19), 40874/40871–40874/40878.
Zheng, Y., Yang, J., Zheng, W., Wang, X., Xiang, C., Tang, L., et al. (2013). Synthesis of flexible magnetic nanohybrid based on bacterial cellulose under ultrasonic irradiation. *Materials Science and Engineering: C*, *33*(4), 2407–2412.
Zhijiang, C., Chengwei, H., Guang, Y., & Jaehwan, K. (2012). Bacterial cellulose as a template for the formation of polymer/nanoparticle nanocomposite. *Journal of Nanotechnology in Engineering and Medicine*, *2*(3), 031006–031006.
Zhou, P., Wang, H., Yang, J., Tang, J., Sun, D., & Tang, W. (2012a). Bacteria cellulose nanofibers supported palladium(0) nanocomposite and its catalysis evaluation in heck reaction. *Industrial & Engineering Chemistry Research*, *51*(16), 5743–5748.
Zhou, P., Wang, H., Yang, J., Tang, J., Sun, D., & Tang, W. (2012b). Bio-supported palladium nanoparticles as a phosphine-free catalyst for the Suzuki reaction in water. *RSC Advances*, *2*(5), 1759–1761.